ACS Infectious Diseases

pubs.acs.org/journal/aidcbc

Article

O-Methylation of the Glycopeptidolipid Acyl Chain Defines Surface Hydrophobicity of *Mycobacterium abscessus* and Macrophage Invasion

Wassim Daher,[‖] Louis-David Leclercq,[‖] Albertus Viljoen, Jona Karam, Yves F. Dufrêne, Yann Guérardel, and Laurent Kremer*

Cite This: *ACS Infect. Dis.* 2020, 6, 2756−2770

Read Online

ACCESS | Metrics & More | Article Recommendations | Supporting Information

ABSTRACT: *Mycobacterium abscessus*, an emerging pathogen responsible for severe lung infections in cystic fibrosis patients, displays either smooth (S) or rough (R) morphotypes. The S-to-R transition is associated with reduced levels of glycopeptidolipid (GPL) production and is correlated with increased pathogenicity in animal and human hosts. While the structure of GPL is well established, its biosynthetic pathway is incomplete. In addition, the biological functions of the distinct structural parts of this complex lipid remain elusive. Herein, the *fmt* gene encoding a putative *O*-methyltransferase was deleted in the *M. abscessus* S variant. Subsequent biochemical and structural analyses demonstrated that methoxylation of the fatty acyl chain of GPL was abrogated in the Δ*fmt* mutant, and this defect was rescued upon complementation with a functional *fmt* gene. In contrast, the introduction of *fmt* derivatives mutated at residues essential for methyltransferase activity failed to complement GPL defects, indicating that *fmt* encodes an *O*-methyltransferase. Unexpectedly, phenotypic analyses showed that Δ*fmt* was more hydrophilic than its parental progenitor, as demonstrated by hexadecane−aqueous buffer partitioning and atomic force microscopy experiments with hydrophobic probes. Importantly, the invasion rate of THP-1 macrophages by Δ*fmt* was reduced by 50% when compared to the wild-type strain. Together, these results indicate that Fmt *O*-methylates the lipid moiety of GPL and plays a substantial role in conditioning the surface hydrophobicity of *M. abscessus* as well as in the early steps of the interaction between the bacilli and macrophages.

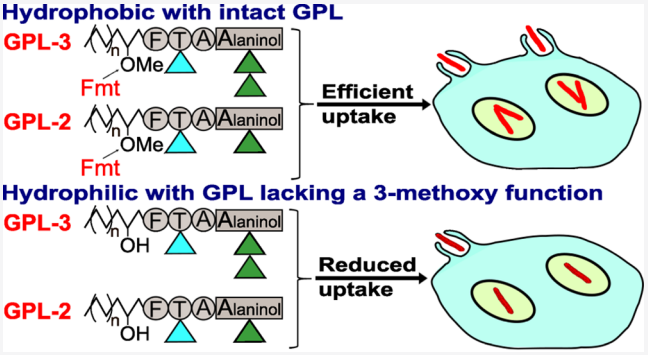

KEYWORDS: *Mycobacterium abscessus, glycopeptidolipid, O-methyltransferase, hydrophobicity, phagocytosis, atomic force microscopy*

Infections caused by nontuberculous mycobacteria (NTM) are increasing globally and are usually difficult to treat due to their inherent resistance to many common antibiotics.[1] Among NTM, *Mycobacterium abscessus* is a fast-growing species and an emerging human pathogen that causes nosocomial skin and soft tissue infections[2] but also pulmonary infections, especially in patients with cystic fibrosis (CF) and other lung disorders.[3,4] Like other NTM, *M. abscessus* exhibits either smooth (S) or rough (R) colony morphotypes, which are associated with distinguishable *in vitro* and *in vivo* phenotypes. This colony-based distinction relies on the production of high (in S) or low (in R) levels of surface-associated glycopeptidolipids (GPLs).[5−7] Comparative genomic and transcriptomic studies have been conducted to better understand the molecular mechanisms responsible for the S-to-R transition in *M. abscessus*, revealing multiple insertions or deletions occurring in the R variants, mainly in the *mps1*, *mps2*, *gap*, and *mmpL4b* genes that are involved in either the synthesis or transport of GPLs.[8] Epidemiological surveys showcased the prominence of the *M. abscessus* R strain in patients with severe pulmonary infections[9,10] and with chronic colonization of the airways in CF patients,[10] underlining that the distinction between S and R morphotypes is of paramount importance and clinically relevant. Indeed, numerous studies have emphasized that the presence or loss of GPL conditions important physiological and physiopathological aspects of infection, among which changes in sliding motility, biofilm formation, and susceptibility to antibiotics have been reported.[5,7,11−13] Other properties related to the GPL content have been disclosed, such as bacterial surface hydrophobicity,[14,15] aggregation leading to cord formation,[5,13,14,16] interaction with and intracellular trafficking in macro-

Received: July 10, 2020
Published: August 28, 2020

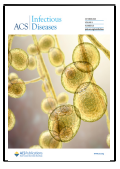

https://dx.doi.org/10.1021/acsinfecdis.0c00490
ACS Infect. Dis. 2020, 6, 2756−2770

phages,[17,18] and induction of a pro-inflammatory response,[19] all influencing the clinical outcome of the disease. This has also been raised by recent studies using various cellular and animal models, confirming the increased pathogenesis of the R over the S form.[13,16,20,21] In particular, the zebrafish model of infection has been proposed as a relevant and genetically tractable host−pathogen conjugate for dissecting *M. abscessus* interactions with host cells,[22] which clearly showed that the S-to-R transition is associated with exacerbation of the bacterial burden, the formation of massive serpentine cords, abscess formation, and increased larval killing.[16] The mycobacterial cell envelope comprises, from the inside to the outside, a plasma membrane surrounded by the peptidoglycan layer, covalently connected to an arabinogalactan layer, which itself is attached to the outermost membrane bilayer, designated the mycomembrane.[23,24] The inner leaflet of this outer membrane is predominantly composed of mycolic acids, while the outer leaflet contains a mixture of free lipids, such as triacylglycerol (TAG) and diacylglycerol (DAG), and a series of complex lipids, including trehalose mono- and dimycolate as well as GPLs. From a structural point of view, GPLs are composed of a lipopeptide ornamented with a flexible arrangement of glycosylation that is built from *O*-methylated and *O*-acetylated deoxy hexoses[18,25,26] (Figure 1A). The peptidic core consists of

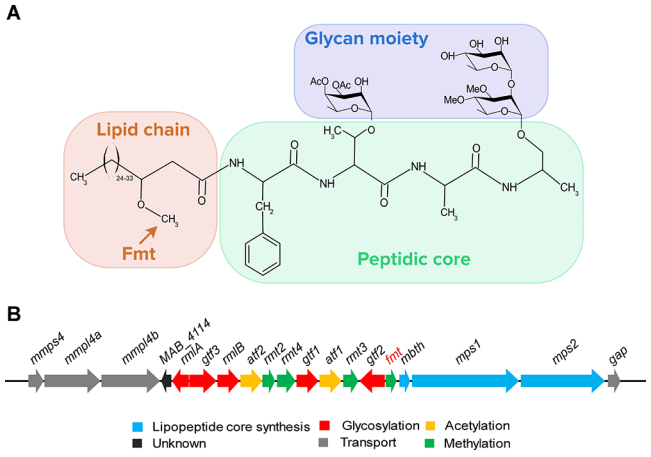

Figure 1. The biosynthetic locus and structure of *M. abscessus* GPL. (A) The lipid, peptidic, and glycan moieties of GPL are indicated by different colors. The schema illustrates the triglycosylated form of GPL (GPL-3) consisting of a D-Phe-D-*allo*Thr-D-Ala-L-alaninol peptidic core (green) of which the D-*allo*Thr is glycosylated with a 3,4-di-*O*-acetyl 6-deoxy-L-talose residue and the alaninol is diglycosylated with rhamnose and 3,4-di-*O*-methylated rhamnose residues. The three monosaccharides are presented in the blue area. The orange arrow shows the methyl group, presumably transferred by the fatty acid *O*-methyltransferase enzyme (Fmt) onto position 3 in the lipid chain (orange area). (B) The GPL locus encodes multiple components required for biogenesis, modification, and transport of the GPL. *fmt* is indicated in orange.

a D-phenylalanine-D-*allo*threonine-D-alanine (D-Phe-D-*allo*Thr-D-Ala) tripeptide linked to an L-alaninol. This D-Phe-D-*allo*Thr-D-Ala-L-alaninol sequence is assembled by two nonribosomal peptide synthetases, Mps1 and Mps2, and acylated with a 3-hydroxy/methoxy C_{24}−C_{33} fatty acid by an unidentified acyltransferase.[26−28] The lipopeptide core is glycosylated with the *allo*-Thr linked to a 6-deoxy-α-L-talose (6-dTal), while the alaninol is linked to an α-L-rhamnose (Rha), producing the less-polar diglycosylated GPL species. In addition to the diglycosylated GPLs that contain a 3,4-di-*O*-acetylated 6-dTal and a 3,4-di-*O*-methylated or 2,3,4-tri-*O*-methylated Rha,[18,26,29] *M. smegmatis* and *M. abscessus* also produce more polar GPLs by the addition of a 2,3,4-trihydroxylated Rha to the alaninol-linked 3,4-di-*O*-methyl Rha.[26,30] Although structurally identical, triglycosylated GPLs are more abundant in *M. abscessus* than in *M. smegmatis*.[26] GPLs are heterogeneous in structure and vary according to the fatty acyl chain length and the degree of hydroxylation or *O*-methylation of the glycosidic moieties through the action of various *O*-glycosyltransferases, *O*-methyltransferases, and *O*-acetyltransferases[31] (Figure 1A). Interestingly, a recent study revealed unexpected structural features of the GPL content in *M. abscessus* grown on CF sputum or synthetic CF medium, consisting of an increase in the amount of triglycosylated forms and possible replacement of the classical carboxy terminal alaninol by other branched-chain aminol alcohols, valinol or leucinol.[32] Despite the relevance of GPLs in NTM of clinical significance, the GPL biosynthetic pathway, which has been well delineated in *M. smegmatis* and *M. avium*,[25,33−36] is only partly described in *M. abscessus*. The individual role of several genes compulsory for GPL production, particularly modifications of the lipid part of the GPL, remains to be experimentally investigated. In addition, whether changes in the acyl chain influence the surface properties of *M. abscessus* and eventually its early interaction with host cells remains undetermined. In this study, we questioned as to whether *fmt*, a gene located within the GPL biosynthetic locus of *M. abscessus* (Figure 1B), participates in GPL biogenesis.

Construction of a genetically deficient *fmt* mutant was used to demonstrate that *fmt* encodes an *O*-methyltransferase. Importantly, deletion of *fmt* abrogated *O*-methylation of the fatty acyl chain of the GPL, which strongly impacted the bacterial surface properties and phagocytosis of *M. abscessus* by human macrophages. Overall, this study advances our understanding of the genetic requirements for the biosynthesis and biological functions of the high-GPL producing variant of this understudied human pathogen.

RESULTS

Loss of *fmt* Affects Neither Growth nor Colony Morphology of *M. abscessus In Vitro*. To get insights into the function of the Fmt protein, conventional gene inactivation was performed in the high-GPL producing *M. abscessus* S variant using an unmarked deletion system.[37] The strategy involves double homologous recombination leading to the removal of the *fmt* open reading frame from the GPL locus (Figure 2A) using the pUX1-*katG* suicide construct, which carries a kanamycin resistance (kan^R) cassette, a tdTomato red fluorescence marker, and a *katG* cassette that confers sensitivity to isoniazid, an antitubercular drug to which *M. abscessus* is naturally resistant.[37] Two DNA sequences flanking *fmt* were cloned adjacently to each other into pUX1-*katG* effectively leading to an *fmt*-deleted allele in the resulting pUX1-*katG*-*fmt* vector. After transformation, clones that integrated pUX1-*katG*-*fmt* into their chromosome *via* a first homologous recombination were isolated by their resistance to kanamycin and their red fluorescence. A subsequent second homologous recombination step resulting in the loss of pUX1-*katG*-*fmt* allowed isolation of potential Δ*fmt* clones by their resistance to isoniazid, loss of red fluorescence, and kanamycin sensitivity. PCR and sequencing screens on genomic DNA using primers listed in Table S1 confirmed the genotype of a

https://dx.doi.org/10.1021/acsinfecdis.0c00490
ACS Infect. Dis. 2020, 6, 2756−2770

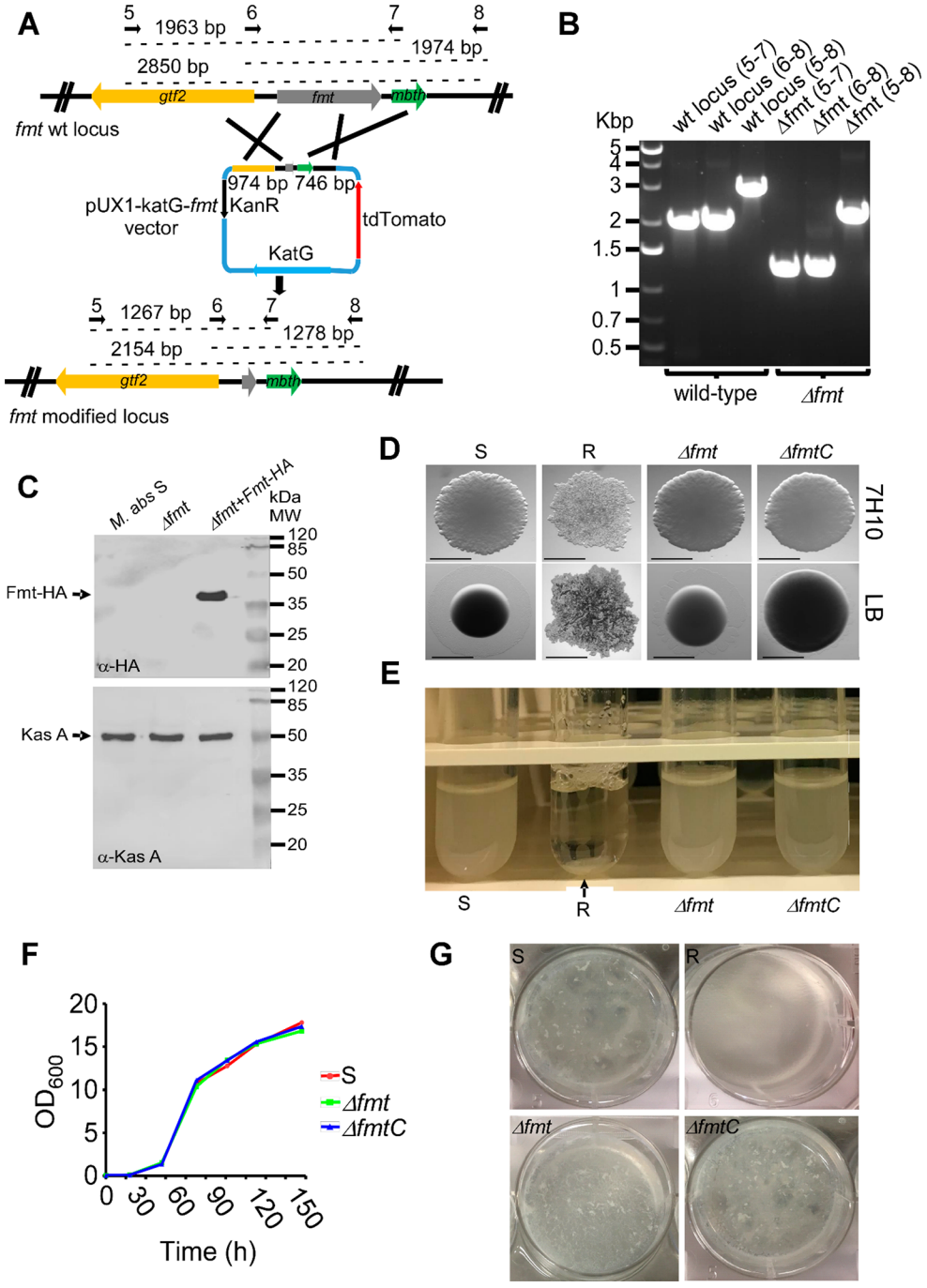

Figure 2. Generation of an unmarked *fmt* deletion mutant in *M. abscessus*. (A) The *fmt* gene is neighbored by the genes *gtf2* and *mbth*. To generate Δ*fmt*, two sequences of 974 and 746 bp located upstream and downstream of *fmt* were cloned into pUX1-*katG*. The resulting suicide plasmid (lacking motifs for episomal replication or mobile elements promoting chromosomal integration) was used to transform *M. abscessus*, in which it could only propagate *via* homologous recombination between the cloned sequences and their chromosomal homologous sequences. The first recombination event was selected in the presence of kanamycin. A single red fluorescent tdTomato-expressing clone was subjected to the second round of recombination selected on isoniazid and screened for double crossover phenotypes, i.e., loss of red fluorescence, sensitivity to kanamycin, and resistance to isoniazid. Dotted lines represent the size (indicated above each line) of the expected PCR products in *M. abscessus* WT and Δ*fmt*. Black arrows represent the primers used for PCR analysis. (B) PCR analysis demonstrating the deletion of *fmt* in the mutant strain. Genomic DNA from WT bacteria was used to amplify the intact *fmt* locus. Amplicons were subjected to sequencing to confirm the deletion of *fmt*. (C) Western blot analysis of the Δ*fmtC* strain expressing the Fmt protein in fusion with an HA tag under the control of the native *fmt* promoter. KasA was included as a loading control. (D) Colony morphology of the S, R, Δ*fmt*, and Δ*fmtC* strains on either 7H10^{OADC} or LB plates. No difference in colony morphology between the progenitor S and Δ*fmt* strains was found, regardless of the media used. Experiments were carried out twice. (E) Like the parental S strain, but unlike the R variant, Δ*fmt* does not sediment rapidly in liquid culture. The arrow indicates the sedimented bacterial aggregates. (F) Growth curve of parental S, Δ*fmt* and Δ*fmtC* strains in 7H9 medium at 37 °C. Data is representative of three independent experiments. (G) Pellicle-forming capabilities of *M. abscessus* S, R, Δ*fmt*, and Δ*fmtC* strains. Experiments were carried out twice.

https://dx.doi.org/10.1021/acsinfecdis.0c00490
ACS Infect. Dis. 2020, 6, 2756−2770

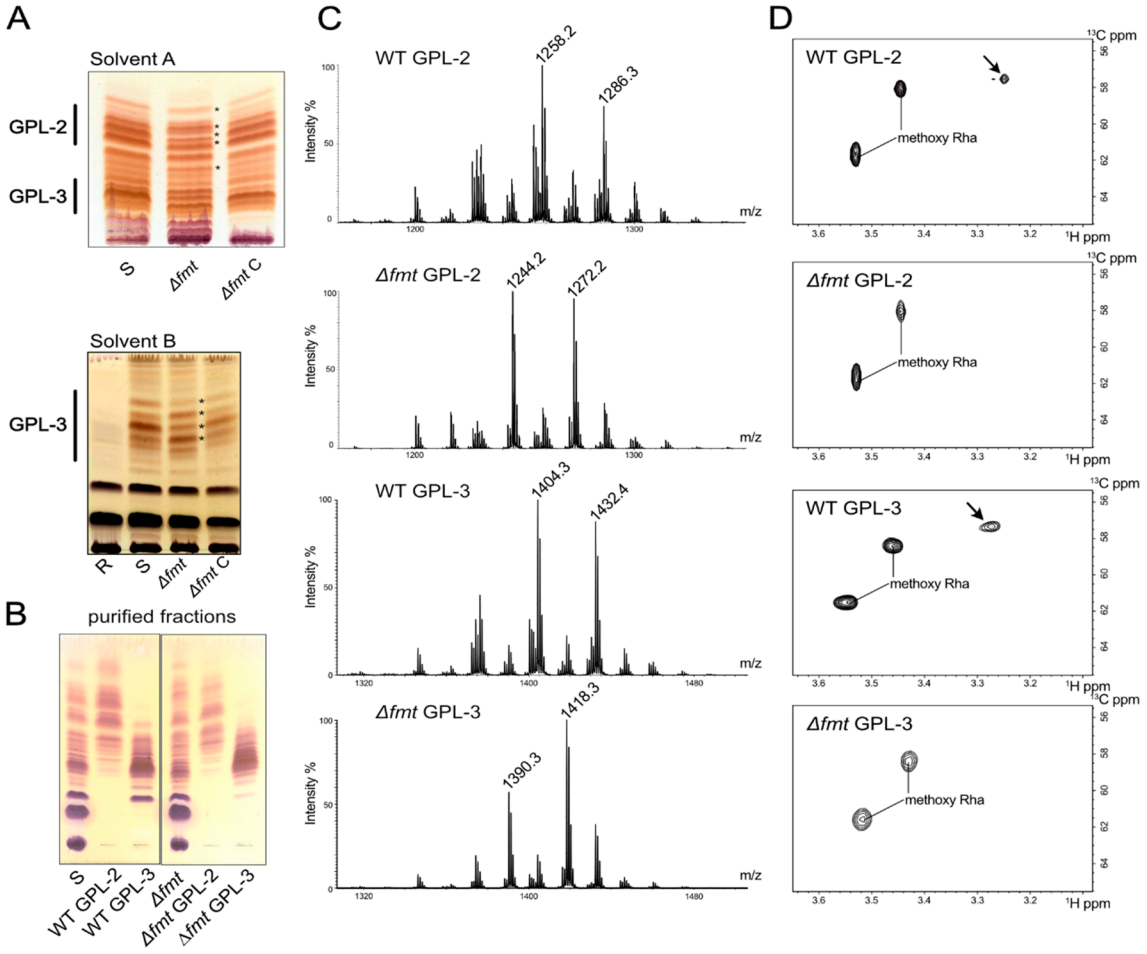

Figure 3. Loss of fatty acid methylation on GPL from Δ*fmt*. (A) TLC analysis of the crude lipid fractions of the parental, mutant, and complemented strains. GPL-2 and GPL-3 were separated using either solvent A ($CHCl_3$/MeOH 95:5, v/v; upper panel) or solvent B ($CHCl_3$/MeOH 9:1, v/v; lower panel) and revealed with orcinol staining after two rounds of migration. GPLs are expressed at similar levels in the parental (S), Δ*fmt*, and Δ*fmtC* strains but are absent in the R variant. Mobility of diglycosylated and triglycosylated GPL species differ in Δ*fmt* as compared to the WT and Δ*fmtC* strains (upper panel). (B) Diglycosylated fractions (GPL-2) and triglycosylated fractions (GPL-3) were separated by flash chromatography and visualized on TLC. (C) MS spectra of GPL-2 and GPL-3. The two upper panels correspond to GPL-2 fractions while the two lower panels correspond to GPL-3 fractions. A decrease of 14 m.u. is observed between WT and Δ*fmt* GPL fractions. (D) $^1H/^{13}C$ HSQC spectra of purified GPL fractions show methoxy functions substituting either the Rha or the lipid moiety. The methoxy group on the lipid moiety is exclusively found on WT GPL-2 and GPL-3 at δ 3.27/57.4 ppm, as indicated by the arrow.

Δ*fmt* mutant (Figure 2B). To confirm that *fmt* alone was responsible for any phenotypic defects observed in Δ*fmt*, the mutant was complemented by site-specific integration at the L5 mycobacteriophage chromosomal attachment site[38] of a C-terminally HA-tagged *fmt* copy under control of its endogenous promoter (Figure 2C). Western blotting was carried out by loading an equal amount of total protein extracts (confirmed by the KasA protein internal loading control). A band with the approximate molecular weight expected for the Fmt-HA protein was detected in the complemented strain, designated Δ*fmtC*.

Since it is well established that the absence or the presence of GPL conditions the morphotype of *M. abscessus* colonies on agar medium, we next assessed whether the disruption of *fmt* influences the morphology of the strain. Serial dilutions of cultures were plated on Middlebrook 7H10 or on LB agar, and single colonies were observed after 4−5 days of incubation. No visual differences in the morphology were noticed between the WT (S morphotype), Δ*fmt*, and Δ*fmtC* colonies, regardless of the medium used; these strains did not show the typical serpentine cords typifying the R variant (Figure 2D). Moreover, Δ*fmt* failed to aggregate in liquid culture but produced homogeneous suspensions similar to *M. abscessus* S cultures (Figure 2E). The *in vitro* growth curves in 7H9 broth at 37 °C were also similar for the S, Δ*fmt*, and Δ*fmtC* strains, indicating that the deletion of *fmt* does not have an impact on the replication rate of *M. abscessus* in planktonic culture (Figure 2F). Along the same lines, like the S progenitor, Δ*fmt* produced fragile pellicles at the air−liquid interface (Figure 2G).

Disruption of *fmt* Alters the Overall GPL Profile in *M. abscessus*. GPLs are a heterogeneous family of polar glycolipids whose structures have been well established in several NTM, including *M. abscessus*.[18,25,26] Individual GPLs comprise three structural parts, a Phe-*allo*Thr-Ala-alaninol peptidic core, a lipid chain, and a glycan moiety. In *M. abscessus*, a C_{24}−C_{33} 3-methoxylated fatty-acyl chain esterifies the amino group of the Phe, while the *allo*Thr and alaninol are substituted by a 6-dTal and by one or two Rha residues, respectively (Figure 1A). The presence of one or two Rha residues differentiates diglycosylated (GPL-2) from triglycosylated (GPL-3) GPL species. The impact of *fmt* deletion on the

https://dx.doi.org/10.1021/acsinfecdis.0c00490
ACS Infect. Dis. 2020, 6, 2756−2770

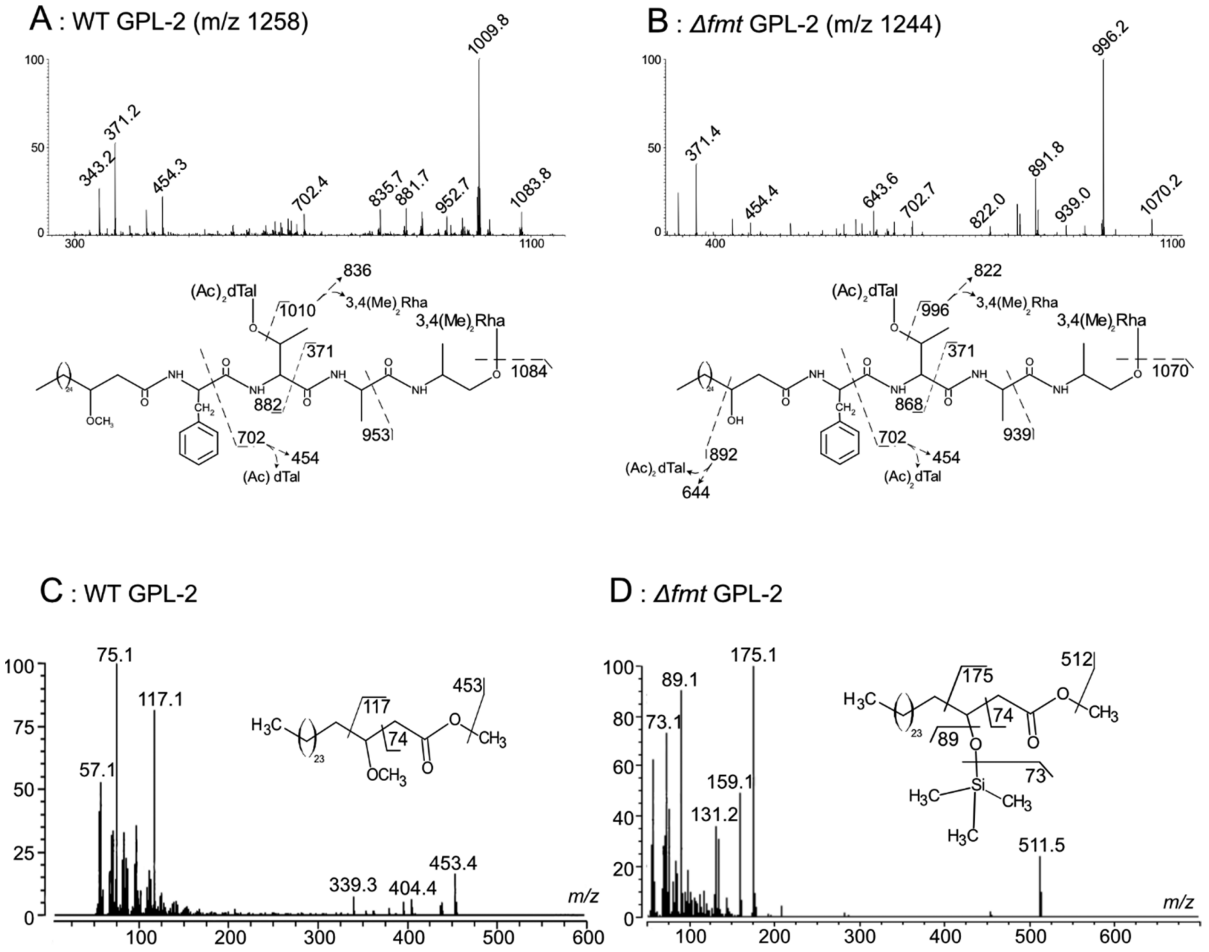

Figure 4. Structural analysis of GPL-2. MS^2 fragmentation spectra of the MS signal (A) at *m/z* 1258 of WT GPL-2 and (B) at *m/z* 1244 of Δ*fmt* GPL-2. EI-MS spectra of (C) 3-methoxylated C_{28} FAMEs isolated from WT GPL-2 and its (D) 3-trimethylsilylated C_{28} equivalent, from Δ*fmt* GPL-2.

overall GPL profile was first analyzed by lipid extraction and separation by thin-layer chromatography (TLC). As anticipated, GPL production was abrogated in the *M. abscessus* R morphotype, whereas the S variant produced large amounts of highly heterogeneous di- and triglycosylated GPL (Figure 3A).[26] Major differences were noticed in the migration profile between the S variant and Δ*fmt*, presumably resulting from small chemical changes in individual molecules. Two rounds of migration showed that the modified GPL pattern in Δ*fmt* comprises GPL species that were either produced in lower amounts or accumulated. Importantly, the wild-type (WT) GPL profile was restored in Δ*fmtC*, indicating that the altered GPL profile cannot be attributed to a polar effect caused by the gene deletion in Δ*fmt*.

To qualitatively analyze GPL-2 or GPL-3 from WT S and Δ*fmt* strains, an in-depth analysis was carried out. Partial purification of the GPL-2 and GPL-3 fractions was accomplished by liquid flash chromatography on a silica gel column and monitored by TLC analysis (Figure 3B). Starting from the lower part of the TLC to the solvent front, two intense and sharp bands, tentatively identified as trehalose-containing lipids with unsaturated C_{16} and C_{18} fatty acids (data not shown), were observed along with multiple bands with higher R_f values, corresponding to GPL-3 and GPL-2, on the basis of their respective mobilities. These fractions were next subjected to thorough structural analyses.

The Glycan Moiety of GPL Is Not Altered in the Δ*fmt* Strain. The monosaccharide composition determined by GC/MS of WT GPL-2 showed the presence of 3,4-di-*O*-methyl Rha and 6-dTal in an approximate 1:1 ratio. Very similar results were obtained with the Δ*fmt* GPL-2 fraction (Figure S1). Both WT GPL-3 and Δ*fmt* GPL-3 showed the presence of 3,4-di-*O*-methyl Rha, 6-dTal, and Rha in an approximate 1:1:1 ratio (Figure S2). In addition, 3-*O*-methyl Rha was observed in much lower quantities on all chromatograms, suggesting the presence of minor glycoforms. These results not only confirm that GPL-3 lipids correspond to extended GPL-2 lipids with an additional Rha residue but also imply that loss of *fmt* does not influence the monosaccharide composition of GPL. Mass spectrometry analysis of GPL-2 and GPL-3 from WT and Δ*fmt* showed complex patterns of signals dominated by two major signals with 28 m.u. increments, tentatively attributed to two CH_2 groups (Figure 3C). The 146 Da increment between WT GPL-2 and WT GPL-3 major signals at *m/z* 1258/1286 and *m/z* 1404/1432 was tentatively attributed to a deoxyhexose, confirming that WT GPL-3 corresponds to WT GPL-2 with an extra Rha residue, in agreement with GC/MS analysis and previous reports.[26,31] The fine sequence of individual WT GPL was further delineated by MS^2 fragmentation of the intense ions at *m/z* 1258 (Figure 4A) and 1404 (Figure S3A). The presence of terminal Me_2Rha and Ac_2dTal residues in WT GPL-2 was established owing to

https://dx.doi.org/10.1021/acsinfecdis.0c00490
ACS Infect. Dis. 2020, 6, 2756−2770

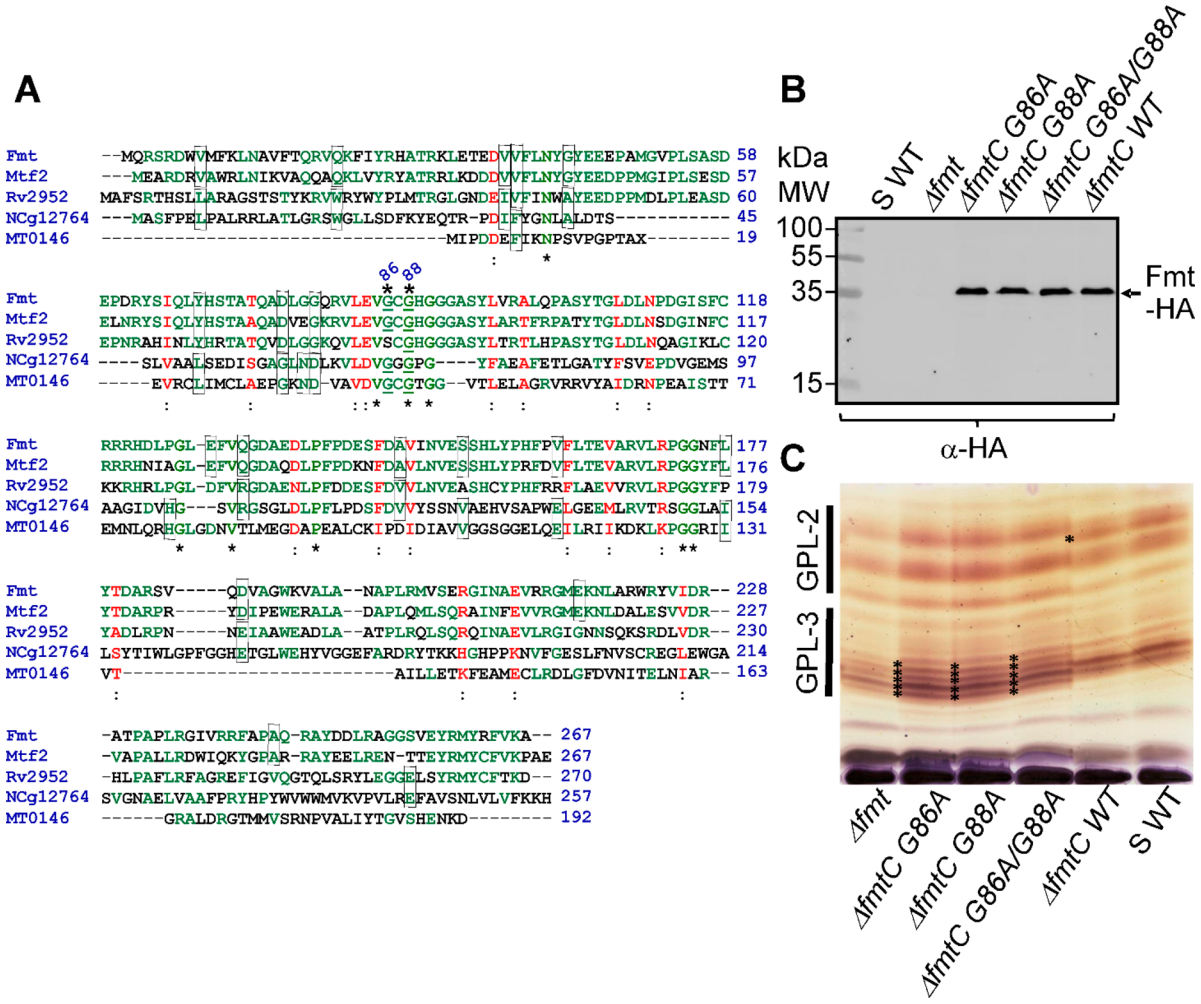

Figure 5. The GXG motif is essential for Fmt activity. (A) Multiple sequence alignment of Fmt with the *Methanobacterium thermoautotrophicum* protein MT0146, the corynebacterial protein NCg12764, the *M. tuberculosis* protein Rv2952, and its orthologue in *M. smegmatis* (Mtf2) using CLUSTALW. Similar residues are shown in red, and identical residues are in green. Wherever possible, the two types of identical amino acids were surrounded within the same vertically aligned column. Conserved glycine residues (Gly86 and Gly88) within the GXG motif and mutated in this study are numbered. (B) Western blot analysis of the Δ*fmt* strain expressing the Fmt(WT)-HA, Fmt(G86A)-HA, Fmt(G88A)-HA, or Fmt(G86A/G88A)-HA fusion proteins under the control of the *fmt* native promoter. (C) TLC analysis of the crude lipid fractions of the parental, mutant, and the various complemented strains. GPLs were separated using $CHCl_3$/MeOH (9:1, v/v) and revealed after spraying with orcinol and charring. Black asterisks indicate modified GPL species.

primary fragment ions at *m/z* 1084 and 1010, respectively, and confirmed by secondary ion products at *m/z* 836 and 454 (Figure 4A). In contrast, WT GPL-3 was characterized by a terminal Rha and Ac_2dTal residues owing to primary fragment ions at *m/z* 1258 and 1156 and to a number of secondary ion products (Figure S3A), confirming that WT GPL-3 was further elongated by a single Rha residue on the Me_2Rha as compared to WT GPL-2. Similar results were obtained on 28 m.u. higher parent ions for GPL-2 and GPL-3 at *m/z* 1286 and 1432, corresponding to a longer lipid chain (data not shown). The presence of the two acetyl groups on dTal residues to form Ac_2dTal was confirmed by MS and MS/MS analyses of mild alkali treated GPL that led to an 84 m.u. decrease for the molecular ion as well as for all fragments containing the dTal residue. This is exemplified by the MS analysis of saponified WT GPL-3 that shows two signals at *m/z* 1319 and 1347 (Figure S4A), as compared to ions at *m/z* 1404 and 1432 for the nontreated fraction (Figure 3C) and confirmed by the corresponding MS/MS fragmentation patterns (Figure S4B).

As for WT, the MS spectra from Δ*fmt* GPL-2 and Δ*fmt* GPL-3 showed complex patterns dominated by major ions with 146 m.u. increments at *m/z* 1244/1272 and *m/z* 1390/1418, respectively, exhibiting a 14 m.u. decrease compared to WT GPL-2 and WT GPL-3 (Figure 3C), tentatively assigned to the loss of a methyl group on Δ*fmt* GPL. MS^2 fragmentation patterns of the major GPL species (Figures 4B and S3B) and of their alkali-treated equivalents (data not shown) established that the glycan moieties of Δ*fmt* GPL-2 and Δ*fmt* GPL-3 were identical to those of WT GPL-2 and WT GPL-3. These results clearly indicate that the deletion of *fmt* does not alter the glycan moiety of GPL.

The Fatty Acyl Chain of GPL Lacks a 3-Methoxy Function in Δ*fmt*. NMR was subsequently used to unambiguously identify the origin of the 14 m.u. decrease in Δ*fmt* samples. In particular, $^1H/^{13}C$ HSQC heteronuclear experiments confirmed that one signal in the region of *O*-CH_3 chemical shifts at δ 3.27/57.4 ppm ($^1H/^{13}C$) detected for WT GPL-2 and GPL-3 was absent in the corresponding Δ*fmt* fractions (Figure 3D). This signal was clearly identified as a

https://dx.doi.org/10.1021/acsinfecdis.0c00490
ACS Infect. Dis. 2020, 6, 2756−2770

methoxy group associated with the fatty acid chain, according to its chemical shifts reported in *M. smegmatis*.[39,40] In contrast, the two less shielded signals, which were similarly observed in all samples, were assigned to the *O*-Me of Me_2Rha, in agreement with previous work.[41] This confirmed that *fmt* has no influence on the methylation of Rha residues. To further certify the loss of methoxylated fatty acids in Δ*fmt*, the fatty acid composition of WT GPL and Δ*fmt* GPL was investigated by GC/MS. As expected, a mixture of methoxylated fatty acids dominated by a C_{28} octacosanoyl form was identified in WT GPL.[40] Electronic-impact mass spectrometry (EI-MS) fragmentation (Figure 4C) of the fatty acid methyl esters (FAMEs) highlighted the presence of a methoxy group in the 3-position owing to the presence of a specific fragment ion at m/z 117. Similar experiments on Δ*fmt* GPL did not permit the identification of similar methoxylated fatty acids. To identify potential nonmethoxylated fatty acids, the free hydroxyl groups of FAMEs extracted from Δ*fmt* GPL were labeled by trimethylsilylation prior to GC/MS analysis. EI/MS of the reaction products from Δ*fmt* GPL showed the presence of C_{28} octacosanoyl FAME hydroxylated in the 3-position owing to the intense fragment ion at m/z 175 (Figure 4D). Finally, exhaustive analysis of MS data of Δ*fmt* GPL-3 revealed that MS^2 spectra of ions at m/z 1390 and 1418 generated a specific fragment ion at m/z 1038, resulting from the cleavage of the fatty acid C3−C4 bond next to the hydroxyl group that could be further fragmented by MS^3 (Figure S5A). This specific fragment ion was not detected in WT GPLs, although an isobaric fragment ion resulting from the cleavage of glycosidic bonds was found by MS^3 analysis (Figure S5B). These data support the view that WT GPLs are substituted by 3-methoxylated fatty acids while Δ*fmt* GPLs are substituted by their hydroxylated equivalents.

The GXG Motif Is Essential for the Methyltransferase Activity of Fmt. To investigate whether *fmt* encodes a methyltransferase, the amino acid sequence of Fmt was aligned with other validated methyltransferases using CLUSTALW (https://www.genome.jp/tools-bin/clustalw). The aligned sequences include MT0146/CbiT from *Methanobacterium thermoautotrophicum*,[42] the corynebacterial MtrP protein (NCg12764) assisting the transport of trehalose mycolates,[43] the methyltransferase catalyzing the transfer of a methyl group onto the lipid moiety of phthiotriol and glycosylated phenolphthiotriol dimycocerosates in *M. tuberculosis* (Rv2952),[44] and the Fmt orthologue in *M. smegmatis* Mtf2,[45] for which active site residues have been identified. In particular, two glycine residues are conserved in *S*-adenosyl methionine (SAM)-dependent methyltransferase and known to be involved in binding to the methyl donor. These correspond to Gly86 and Gly88 in Fmt, which are also conserved in MT0146/CbiT, NCg12764, and Mtf2 (Figure 5A). However, only the second glycine residue is conserved in Rv2952 (Figure 5A). We reasoned that, if replacement of these crucial residues by Ala would result in loss of methoxylation, *trans*-complementation of Δ*fmt* with the Ala mutated *fmt* alleles would fail to restore the WT GPL pattern. Thus, Δ*fmt* was transformed with constructs allowing expression of Fmt variants (HA-tagged) in which Gly86 and Gly88 were either individually or simultaneously substituted by Ala. The introduction of pMV306-*fmt*-G86A, pMV306-*fmt*-G88A, or pMV306-*fmt*-G86A/G88A into Δ*fmt* resulted in similar expression levels of the different Fmt variants, as judged by probing the proteins with anti-HA antibodies (Figure 5B). The TLC profile of the extracted lipids clearly indicates that the introduction of the single or double mutations in *fmt* failed at functionally complementing the GPL profile (Figure 5C).

To support these results, GPL-2 and GPL-3 were purified from Δ*fmt* harboring pMV306-*fmt*-G86A, pMV306-*fmt*-G88A, or pMV306-*fmt*-G86A/G88A and analyzed by MS. As depicted in Figure S6 and in agreement with the TLC pattern, the MS profiles in these three strains remain identical with the one in Δ*fmt*. In each of the three Δ*fmt* strains expressing a catalytically inactivated Fmt variant, GPL-3 fractions displayed a set of intense bands with lower R_f due to a more polar behavior (Figure S6A) and identical MS spectra to Δ*fmt*, with two main ions at m/z 1390 and 1418 (Figure S6C). MS^3 analysis of the fragment ion 1418 → 1038 generated very similar fragmentation pattern to those observed for Δ*fmt* GPL-3 (Figure S5A), strongly suggesting the presence of a β-hydroxyl group on the fatty acid (Figure S7). In addition, the two major ions at m/z 1244 and 1272 were found in the GPL-2 fractions of all three strains (Figure S6B). These results establish the absence of methoxylated GPL in Δ*fmt* producing the catalytically inactivated Fmt proteins. Collectively, this indicates that both Gly86 and Gly88 are required for restoring the GPL profile to the WT level and confirm that Fmt is a canonical methyltransferase.

Hydrophobicity of *M. abscessus* S Is Dependent on GPL Methylation. Partitioning of mycobacterial cultures between hexadecane and an aqueous buffer has been used as a quantitative marker of hydrophobicity in *M. tuberculosis* evolution and pathogenicity, ranging from the hydrophilic environmental low-pathogenicity ancestors *Mycobacterium kansasii* and *Mycobacterium canettii* to highly hydrophobic virulent tubercle bacilli.[46] To address whether the methylation of GPL affects the surface hydrophobicity of *M. abscessus*, hexadecane−aqueous buffer partitioning was applied to the S, R, Δ*fmt*, and Δ*fmtC* strains. *M. kansasii* Hauduroy (ATCC 12478) was included as a highly hydrophilic control strain.[46] Consistent with previous findings, the S variant is more hydrophilic than the R variant, while *M. smegmatis* mc^2155 exhibited an intermediate phenotype.[14] Unexpectedly, Δ*fmt*, while producing normal levels of GPL but lacking the methoxy on the fatty acid core, was significantly more hydrophilic than the S variant, almost reaching levels of *M. kansasii*, while complementation restored the wild-type hydrophobic properties of the S strain (Figure 6A). This suggests that lack of *O*-methylation is responsible for the increased hydrophilicity of Δ*fmt*.

Hydrophobic Forces Are Weaker within Hydrophobic Nanodomains on Single Δ*fmt* Cells. Atomic force microscopy (AFM) with chemically modified (hydrophobic) AFM tips was employed to assay at high spatial resolution the magnitudes, frequencies, and surface distributions of hydrophobic adhesive forces on the surface of Δ*fmt*.[15,47] Low resolution topographic images (5 μm × 5 μm) were first recorded, and then, high-resolution adhesion maps were obtained (250 nm × 250 nm, Figure 6B, blue squares) on top of the bacteria to avoid edge artifacts. In line with previous work,[15] heterogeneous distributions of hydrophobic adhesive forces were observed, i.e., hydrophobic nanodomains surrounded by hydrophilic areas on the surface of *M. abscessus* S cells (Figure S8A) as well as on Δ*fmt* (Figure S8B) and Δ*fmtC* cells (Figure S8C). The frequencies of detectable hydrophobic forces on Δ*fmt* (24 ± 3%, n = 19 cells) did not differ significantly from those on WT bacteria (16 ± 4%) or Δ*fmtC*

https://dx.doi.org/10.1021/acsinfecdis.0c00490
ACS Infect. Dis. 2020, 6, 2756−2770

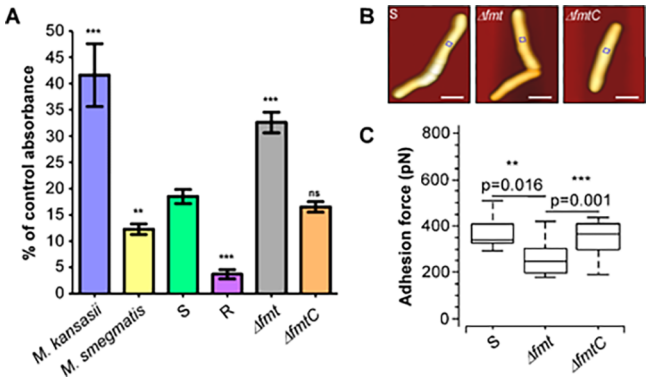

Figure 6. Decreased cell-surface hydrophobicity of Δ*fmt*. (A) *M. abscessus* R is more hydrophobic than S, while the Δ*fmt* mutant strain's hydrophilicity is significantly higher than S, as assessed by hexadecane partitioning and shown as the hydrophobicity index (in percentage of aqueous phase OD prior to partitioning). Histograms and error bars are means ± SD of three independent experiments. Differences between means were analyzed for significance using a two-tailed Student's *t*-test employing Welch's correction for unequal variances. ns, nonsignificant; $^{**}p < 0.01$; $^{***}p < 0.001$. (B) 3D projections of height images obtained in the quantitative imaging (QI) mode of *M. abscessus* S (WT), Δ*fmt*, and Δ*fmtC* cells. The blue squares (250 nm × 250 nm) in each image indicate where adhesion force maps were collected for these representative cells, shown in Figure S8 (WT #2, Δ*fmt* #5, and Δ*fmtC* #1). Scale bar = 1 μm. (C) Boxplots of adhesion forces for *M. abscessus* S wild-type (WT), Δ*fmt*, and Δ*fmtC* cells. Whiskers indicate the range; the bottom and top of the boxes are the 1st and 3rd quartiles, respectively, and the thick black bar in the middle of the boxes represents the sample median. The different groups were compared using one-way Mann−Whitney tests. $n = 17$ (WT); $n = 18$ (Δ*fmt*); $n = 11$ (Δ*fmtC*).

cells (23 ± 4%), indicating that abrogation of GPL methylation by Fmt does not change the proportion of hydrophobic versus hydrophilic areas on the cell surfaces.

To test whether changes in the methylation pattern of GPL affect hydrophobic adhesion within nanodomains, we assessed the average magnitudes of adhesion forces within these domains only (i.e., excluding nonadhesive events). The average adhesion force within hydrophobic nanodomains on Δ*fmt* was 281 ± 28 pN (mean ± SEM, $n = 17$, 481 curves from 18 cells), while in WT cells, it was 375 ± 37 pN (mean ± SEM, $n = 11$, 476 curves from 17 cells), a moderate (~25%) but significant difference ($p = 0.016$). In Δ*fmtC*, adhesive forces with hydrophobic nanodomains were restored to WT levels (371 ± 20 pN, mean ± SEM, $n = 10$, 495 curves from 11 cells). These results shown as boxplots in Figure 6C indicate that the alteration of the GPL methoxylation pattern correlates with changes in the surface hydrophobic properties of *M. abscessus* S cells. It also supports the view that more hydrophobic classes of GPL define the hydrophobic nanodomains exhibited on the surfaces of S variant cells (at least in contribution with other apolar lipid classes). However, the ratio of hydrophobic to hydrophilic area did not change in Δ*fmt*, indicating that methoxylation is not the only determinant of GPL hydrophobicity and that other chemical differences between the class of GPL that define the hydrophilic nanodomains and those that define the hydrophobic ones likely exist.

Reduced Invasion of THP-1 Macrophages by Δ*fmt*. Because cell surface hydrophobicity plays important roles such as favoring cell−surface interactions with host tissues,[48] the first step leading to infection, we next evaluated the possible impact of GPL methylation on adhesion and invasion of *M. abscessus* by human THP-1 macrophages. Cells were infected with the tdTomato-expressing *M. abscessus* S, Δ*fmt*, or Δ*fmtC* strains for 3 h at a multiplicity of infection (MOI) of 2:1, prior to assessing phagocytosis and rate of replication over time. Following infection, macrophages were treated with 250 μg/mL amikacin for 2 h and then amikacin was maintained at 50 μg/mL to prevent extracellular bacterial growth. At 0, 1, 3, and 5 days postinfection (dpi), macrophages were lysed and plated to determine the intracellular bacterial burden. At day 0 (3 h postinfection), the invasion rate of Δ*fmt* was reduced by almost 50% as compared with the control strain, and this effect was rescued with Δ*fmtC* (Figure 7A). This defect was

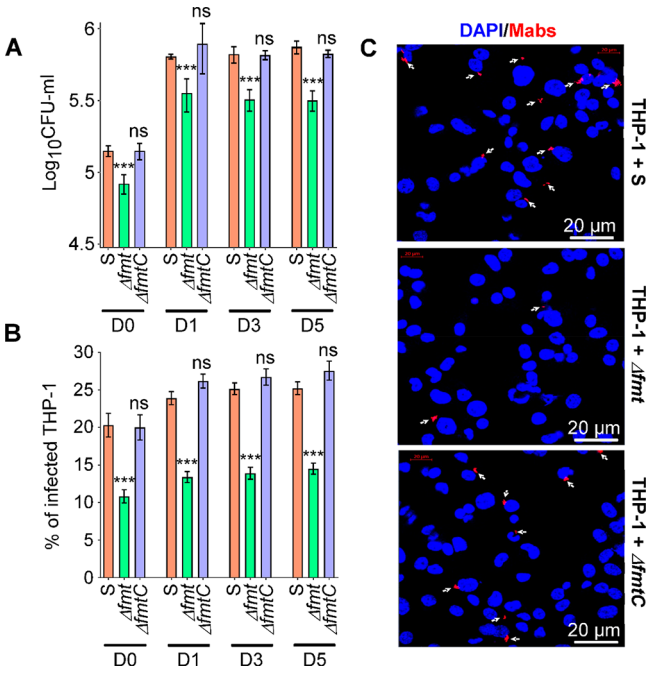

Figure 7. Fmt participates in the invasion of human macrophages by *M. abscessus*. Macrophages were infected with the *M. abscessus* S, Δ*fmt*, and Δ*fmtC* strains expressing tdTomato (MOI of 2:1). (A) CFU were determined at days 0, 1, 3, and 5 postinfection. Data are mean values ± SD for three independent experiments. One-tailed Mann−Whitney test: ns, nonsignificant; $^{***}p < 0.001$. (B) Percentage of infected THP-1 macrophages at days 0, 1, 3, and 5 postinfection. Data are mean values ± SD for three independent experiments. One-tailed Mann−Whitney test: ns, nonsignificant; $^{***}p < 0.001$. (C) Three immunofluorescent fields were taken after 1 day postinfection at a 40× magnification (using a confocal microscope), showing the nuclei of macrophages infected with the various strains. The nuclei are shown in blue. White arrows indicate mycobacteria within the macrophages. Scale bars represent 20 μm. Experiments were done three times independently.

maintained at 1, 3, and 5 dpi (Figure 7A). In parallel, at 0, 1, 3, and 5 dpi, macrophages were stained with DAPI and observed under an epifluorescence microscope. Microscopic observations and quantification of the infected cells revealed a pronounced reduction in the number of infected THP-1 cells infected with Δ*fmt* just after phagocytosis. Again, this effect was maintained over time as compared to the macrophages infected with either the WT progenitor or Δ*fmtC* strains (Figure 7B,C). In contrast, no major effect on bacilli multiplication was observed within the cells, suggesting that

https://dx.doi.org/10.1021/acsinfecdis.0c00490
ACS Infect. Dis. 2020, 6, 2756−2770

fmt is important for bacterial invasion rather than for intracellular survival.

DISCUSSION

This work provides a first glimpse into the structure−function relationship of GPL fatty acid methoxylation. It unambiguously demonstrates that *fmt* encodes a *O*-methyltransferase that catalyzes the transfer of a methyl to the 3-hydroxyl group of the C_{24}−C_{33} fatty acyl chain, with which the amino group of the peptidic core is esterified: (i) unmarked deletion of *fmt* leads to the production of GPL carrying a fatty acyl chain lacking a 3-methoxy group while the glycan moiety remains unaltered; (ii) substitution of the Gly86 and/or Gly88 residues of the conserved GXG motif, known to bind to the methyl donor in other *O*-methyltransferases,[43] resulted in the loss of *O*-methylation of the lipid domain of GPL; (iii) Fmt is the orthologue of Mtf2 that methylates the GPL in *M. smegmatis*.[45] However, because *M. smegmatis* is a nonpathogenic species, the impact of lipid *O*-methylation in the physiopathology of infection cannot be investigated. In addition, we procure strong evidence that *O*-methylation of the GPL fatty acid increases cell surface hydrophobicity of *M. abscessus* and increases internalization of the bacilli by macrophages. By substituting the endogenous promoter of the *mmpS4 mmpL4a-mmpL4b* locus involved in the transport of the GPL with a leaky acetamidase promoter from *M. smegmatis* in *M. abscessus* S, we previously reported a strain producing low GPL levels with a rough appearance, similar to R strains.[14] This rough low GPL producing mutant was less hydrophilic than the S variant but more hydrophilic than the R variant, indicating that lowering the production of GPL leads to increased hydrophobicity. Herein, we show that *O*-methylation of the lipid core of GPL represents another way for *M. abscessus* to regulate its surface hydrophobicity properties. However, these alterations in the GPL profile were not associated with changes in the susceptibility to cefoxitin, imipenem, bedaquiline, amikacin, or rifabutin (data not shown), indicating that methoxylation of the fatty acyl chain does not contribute to the envelope permeability and drug sensitivity of *M. abscessus*.

Earlier comparative studies between the S and R morphotypes of *M. abscessus* underscored the positive correlation between low GPL production and increased hydrophobicity and virulence in animal models.[14] These features are reminiscent of the role that hydrophobicity has played in *M. tuberculosis* evolution toward greater pathogenicity, where more modern pathogenic strains exhibit a higher proportion of less polar lipids in the outer membrane, which corresponds with greater surface hydrophobicity.[46] Importantly, increased hydrophobicity may enhance the capability for aerosol transmission, affecting virulence and pathogenicity.[46,49] Conversely, *M. kansasii*, which is much less pathogenic than *M. tuberculosis* and less virulent than *M. abscessus* in the zebrafish model of infection,[50] produces large quantities of hydrophilic lipids and is characterized by mycomembrane lipids that are less apolar than those found in *M. tuberculosis*.[46] Our results indicate that *M. abscessus* S is less hydrophilic than *M. kansasii* but more than the R morphotype. Remarkably, Δ*fmt* is more hydrophilic than the S parental strain, indicating that a simple change in the methoxylation pattern of GPL can lead to pronounced phenotypic changes in surface hydrophobicity. However, considering the wide heterogeneity of the microbial population in planktonic cultures, comprising a mixture of bacteria with various degrees of hydrophilicity, we aimed at imaging and quantifying surface hydrophobicity at the single cell level using AFM. As noticed previously, the *M. abscessus* S cell surface is characterized by hydrophilic nanodomains, the latter being completely absent in R variant cells that express homogeneous surface hydrophobicity,[15] like in other GPL-defective mycobacteria.[47,51,52] While the homogeneous hydrophobicity on the R variant cell surface is easily explained by the exposure of more hydrophobic lipid classes, like mycolic acids, in the absence of GPL, two explanations for the presence of both hydrophobic and hydrophilic nanodomains on S variant cells were posited: (i) mycolic acids that are hydrophobic (most likely along with other hydrophobic lipids) define the hydrophobic nanodomains, while GPLs, which expose relatively hydrophilic head groups, define the hydrophilic nanodomains; (ii) more hydrophobic GPL classes define the hydrophobic nanodomains, while hydrophilic nanodomains are defined by more hydrophilic classes.[15] The average adhesion force within hydrophobic nanodomains on Δ*fmt* was lower than in the parental and Δ*fmtC* strains, which supports the latter hypothesis. It is possible that more apolar GPL-2 define the hydrophobic nanodomains and that a loss of fatty acid methoxylation leads to decreased hydrophobic adhesive forces measured specifically within hydrophobic nanodomains of Δ*fmt*. Ensuing studies may explore the contribution of the GPL glycosylation profile on surface hydrophobicity.

The fatty acid core of GPL is thought to interact with other lipids present within the outer leaflet of the outer membrane, implying that the methoxy substituent is likely to be buried within the membrane and, presumably, not exposed on the bacterial surface. One cannot, however, exclude that the overall reduced hydrophobicity of Δ*fmt* GPL relies simply on the direct consequence of the lack of the methoxy group. It is possible that this methoxy group is important for the GPL to interact with other membrane lipids. The loss of the methyl group in Δ*fmt* may, therefore, result in "abnormal" interactions with lipids, favoring the exposition of other polar lipids at the bacterial surface, thus influencing the overall cell surface chemical composition and hydrophobic properties. Interestingly, methoxylation has been ascribed to the phenolglycolipids (PGL) and phthiocerol dimycocerosate (PDIM) in *M. tuberculosis*, two other well-described, complex, virulence lipids.[53] In these lipids, the transfer of a methyl group onto the free hydroxyl group of the lipid domain of PDIM and PGL is catalyzed by the methyltransferase Rv2952,[44] whose gene is found within the PDIM/PGL locus, similarly to how *fmt* is located within the GPL locus. Multisequence alignments indicated an overall conservation between Fmt and Rv2952, albeit the GXG motif is not fully conserved in Rv2952 as the first Gly residue is substituted by a Ser. On the basis of our findings with GPL, it would be interesting to investigate whether the lack of lipid methoxylation in PDIM and PGL translates into altered biological properties and influences the pathogenesis of *M. tuberculosis*.

The outermost layer of *M. abscessus* characterizes the interface between bacilli and their host macrophages. It is now clear that the hydrophobic effect is a factor in adhesion of numerous pathogens.[48] Mycobacterial exposed adhesins are recognized by specific cell surface receptors that allow bacteria to reach and invade their cellular targets. A few adhesins have been shown to play a role in the interaction between mycobacteria and host cells, but their surface position and their approachability to their cognate receptors remain poorly

https://dx.doi.org/10.1021/acsinfecdis.0c00490
ACS Infect. Dis. 2020, 6, 2756−2770

understood. This work shows that the decreased cell surface hydrophobicity of Δ*fmt* correlates with reduced invasion of macrophages by *M. abscessus*, while the intracellular growth rate of the mutant was not altered as compared to the one of the WT progenitor. These findings are consistent with previous studies demonstrating that internalization of *M. smegmatis* by human macrophages is more efficient in a mutant lacking GPL (*mps*-inactivated) than in a control strain producing GPL.[29,54] However, whether the reduced adhesion and internalization of Δ*fmt* in macrophages is a direct or indirect effect of the lack of GPL methoxylation deserves future investigations. One possibility could be that GPL are direct ligands of macrophage receptors and that the methoxy of the GPL fatty acid chain participates in the ligand−receptor recognition. Improved adherence to target cells is directly correlated with increased bacterial surface hydrophobicity in *Neisseria* and *Streptococci*.[55,56] Methylation has also been found to increase hydrophobicity of the outer surface of the flagellar filament in *Salmonella* and, consequently, enhance bacterial adhesion and host cell invasion.[57] Additional work is required to understand how bacterial surface hydrophobicity can alter the adhesion strength between bacteria and host cells.

CONCLUSION

This study underscores the contribution of GPL methoxylation in the biological functions of this important class of lipids. Because GPLs are present in numerous NTM, these results suggest that the activity of Fmt participates in the surface properties and internalization of other NTM, highlighting possible therapeutic interventions against these opportunistic mycobacterial pathogens. Future studies should enlighten the contribution of the other parts of this complex lipid molecule with respect to their biological functions.

METHODS

Mycobacterial Strains, Growth Conditions, and Reagents. All bacterial strains are listed in Table S2. Rough (R) and smooth (S) variants of *M. abscessus* CIP104536^T were usually grown in Middlebrook 7H9 broth (BD Difco) supplemented with 0.05% Tween 80 and 10% oleic acid, albumin, dextrose, catalase (OADC enrichment; BD Difco) (7H9$^{T/OADC}$) at 37 °C in the presence of antibiotics, when required. Electro-competent mycobacteria were transformed using a Bio-Rad Gene pulser (25 μF, 2500 V, 800 Ohms). For bacterial selection, media were supplemented either with 1 mg/mL hygromycin for strains carrying pTEC27 (Addgene, plasmid 30182), allowing tdTomato expression, or with 250 μg/mL kanamycin when harboring the pMV306 derivatives. On plates, colonies were selected either on Middlebrook 7H10 agar (BD Difco) supplemented with 10% OADC enrichment (7H10^{OADC}) or on LB agar. Antibiotics were purchased from Sigma-Aldrich.

***In Vitro* Growth, Colony Morphology Assays, and Sedimentation.** Growth was examined by inoculating the mid-log phase cultures into fresh 7H9 at an OD_{600} of 0.05. Cultures were incubated at 37 °C with shaking, and OD_{600} was monitored for 150 h using a Synergy H1 hybrid reader (BioTek). To evaluate colony morphology, bacteria from a log phase bacterial culture (OD_{600} = 1) were resuspended in phosphate buffered saline (PBS) and 2 μL of the cell suspension was spotted onto 7H10^{OADC} or LB agar. Plates were then incubated for 4−5 days at 37 °C, and colonies were imaged using a Zeiss microscope equipped with a Zeiss Plan Neo Fluor Z 1×/0.25 FWD objective. Images were acquired with an Axiocam503 monochrome (Zeiss) camera and processed using ZEN 2 (blue edition). For sedimentation experiments, cultures were diluted to an OD_{600} of 1 and 2 mL of culture were transferred to a glass tube. Images were taken after 5 min.

Pellicle Assays. Pellicle formation was assessed by inoculating 10 μL of mid-log phase mycobacterial cells (OD_{600}, 0.8−1.0) onto medium consisting of M63 supplemented with 10% glucose, 1 mM $CaCl_2$, and 1 mM $MgSO_4$, and the samples were incubated without agitation at 30 °C for 5 days.

Hexadecane Partitioning. Exponentially growing bacteria were washed twice in PUM buffer (100 mM K_2HPO_4, 54 mM KH_2PO_4, 30 mM urea, 0.8 mM $MgCl_2$) and suspended to an OD_{600} of 0.7. Aliquots (3 mL) were transferred to glass tubes, and hexadecane (2.4 mL) was added. After a brief mixing, samples were incubated for 8 min at 37 °C, and phase separation was allowed to occur at 22 °C for 15 min. The hydrophobicity index was defined as aqueous phase OD_{600}, expressed as a percentage of that of the bacterial suspension in PUM buffer alone.[46]

Construction of Δ*fmt*. The suicide vector pUX1-*katG*[37] was used to generate pUX1-*katG-fmt* (Table S3), which was subsequently used to generate an unmarked deletion mutant in the S variant of *M. abscessus*. Briefly, the left and right arms (LA and RA, respectively) were PCR-amplified using genomic DNA and Q5 polymerase (New England Biolabs) as well as primers 1 and 2 (LA) and primers 3 and 4 (RA) (Table S1). The purified LA and RA amplicons were restricted with PacI/MfeI and MfeI/NheI, respectively, and ligated to the PacI-NheI-linearized pUX1-*katG*, yielding pUX1-*katG-fmt*, designed to delete 696 bp (87%) of the *fmt* gene. Electro-competent *M. abscessus* was transformed with pUX1-*katG-fmt*. The selection of bacteria having undergone the first homologous recombination event was done by visual screening of red fluorescent colonies on 7H10^{OADC} supplemented with 250 μg/mL kanamycin. After subculturing the culture overnight in 7H9$^{T/OADC}$ in the absence of kanamycin, bacterial suspensions were serially diluted and plated onto 7H10^{OADC} with 50 μg/mL isoniazid (INH) to select for INH-resistant, Kan-sensitive, and nonfluorescent colonies. The DNA junctions were subsequently PCR sequenced to confirm the proper Δ*fmt* genotype.

Complementation Constructs. Plasmids for complementation were generated by PCR amplification of *fmt* in fusion with an HA tag sequence under the control of its endogenous promoter region (175 bp) using genomic DNA and the forward primer 9 (containing a *Kpn*I site) and reverse primer 10 (containing an NcoI site as well as the HA-coding sequence) and subsequent ligation into the integrative vector pMV306 cut with *Kpn*I and NcoI, resulting in pMV306-*fmt*. The mutation of the Gly86 or/and Gly88 present in the GXG motif in Fmt in pMV306-*fmt* was achieved by site-directed mutagenesis using the primers listed in Table S1 and the QuikChangeV Site-Directed Mutagenesis Kit (Agilent), according to the manufacturer's instructions, yielding pMV306-*fmt*-G86A, pMV306-*fmt*-G88A, and pMV306-*fmt*-G86A/G88A. All constructs were verified by DNA sequencing and introduced into Δ*fmt*.

Western Blotting. Bacteria were harvested, resuspended in PBS, and disrupted by bead beating using 1 mm diameter glass

https://dx.doi.org/10.1021/acsinfecdis.0c00490
ACS Infect. Dis. 2020, 6, 2756−2770

beads. Protein concentration was assessed using the BCA Protein Assay Reagent kit (Pierce), according to the manufacturer's instructions. Equal amounts of proteins (50 μg) were separated by SDS/PAGE and transferred to a nitrocellulose membrane. For detection of Fmt-HA, Fmt-G86A-HA, Fmt-G88A-HA, and Fmt-G86A/G88A-HA, membranes were probed for 1 h with rat anti-HA antibodies (dilution 1:2000; Sigma). The KasA protein, used as an internal loading control, was revealed using rat anti-KasA antibodies (dilution 1:2000).[58] After washing, membranes were incubated for 45 min with goat anti-rat antibody conjugated to HRP (dilution 1:5000; Abcam). The signal was revealed using the ChemiDoc MP system for imaging and analyzing gels (Bio-Rad laboratories).

AFM Tip Functionalization, Sample Preparation, Parameters, and Analysis. Gold OMCL-TR400PB-1 AFM probes (Olympus) were functionalized by immersing them in a 1 mM ethanolic solution of 1-dodecanothiol overnight and used fresh. Bacteria were first cultured in 7H9 broth supplemented with 0.2% (w/v) glucose, 0.2% glycerol, and 0.025% tyloxapol. At the middle exponential phase (OD_{600} ~ 1.0), bacteria were pelleted by centrifugation, resuspended in medium lacking tyloxapol, and deaggregated *via* passing them 10× through a 26 GA syringe needle and finally passing them through a 5 μm PVDF syringe filter (Merck), resulting in a suspension of single bacterial cells. This suspension was seeded into a 35 mm hydrophobic (untreated) microscopy dish (iBidi), and bacteria were left to adhere to the hydrophobic surface overnight at 30 °C. Just prior to AFM measurements, the bacteria were washed several times with deionized water, and all AFM experiments were performed in ultrapure deionized water. Topographic images were recorded in quantitative imaging (QI) mode using a JPK NanoWizard 4 AFM, bare MSCT probes (k = 0.02), and the following parameters: an applied force of 250 pN, 25 μm/s approach and retraction speeds, a z-length of 500 nm, a map size of 5 × 5 μm, and a resolution of 128 × 128 pixels. Adhesion maps were also recorded in QI mode but using hydrophobic probes (k = 0.02) and the following parameters: 25 μm/s approach and retraction speeds, an applied force of 500 pN, a z-length of 500 nm, a map size of 250 nm × 250 nm, and a resolution of 64 × 64 pixels. Owing to tip-geometry induced artifacts that occur on the steep edges of the cells, care was taken to record adhesion maps right on top of the bacteria (250 nm × 250 nm areas). The spring constants of AFM probes were determined empirically using the method of Hutter and Bechhoefer.[59] At least two different tips were used to collect data for each sample, and the AFM experiment was repeated on one occasion. Force−distance curves obtained in QI mode were treated using the JPK Data Processing software (V.6.1.125).

Macrophage Infection Assays. THP-1 macrophages were grown, infected with the *M. abscessus* S, Δ*fmt*, and Δ*fmtC* strains, and processed as reported earlier.[60] At various time points (0, 1, 3, and 5 days postinfection), macrophages were washed three times with PBS and lysed with 100 μL of 1% Triton X100. Cell lysis was stopped by adding 900 μL of PBS, and serial dilutions were plated to monitor the intracellular bacterial counts. Colonies were counted after 5 days of incubation at 37 °C. Microscopy-based infectivity assays were performed as reported previously.[60] Briefly, THP-1 cells were cultivated on coverslips in 24-well plates at a density of 10^5 cells/well. The following day, cells were infected with tdTomato expressing *M. abscessus* (MOI = 2). At various time points after infection, cells were fixed with 4% paraformaldehyde in PBS for 20 min, stained with 1 μg/mL 4′,6-diamidino-2-phenylindole (DAPI) for 5 min, washed, mounted onto microscope slides using Immu-Mount (Calbiochem), and examined using a confocal microscope (63× objective) (Zeiss LSM880). Images were acquired and captured on a Zeiss Axioimager confocal microscope equipped with a 63× oil objective and a camera and processed using Zeiss Axiovision software. Quantification and scoring of the numbers of bacilli present within macrophages were performed within focus using ImageJ. Equal parameters for the capture and scoring of images were consistently applied to all samples. For each condition, ~1000 infected macrophages were analyzed.

GPL Extraction. Bacteria grown on $7H10^{OADC}$ agar plates without detergent were collected, and GPLs were extracted from the polar lipid fraction, first with chloroform/methanol/0.3% NaCl (9:10:3, v/v/v) and then by chloroform/methanol/0.3% NaCl (5:10:4, v/v/v). The combined solvent extracts were then mixed for 5 min with chloroform and 0.3% NaCl (1:1, v/v) and centrifuged at 3000*g* for 5 min to separate the lower-organic phase from the aqueous phase. The upper aqueous layer was discarded, and the lower-organic phase was evaporated under a stream of nitrogen and resuspended in chloroform/methanol (2:1, v/v). Polar lipids were then subjected to TLC analysis using Silica gel 60 F_{254} plates (Merck). GPLs were separated using either chloroform/methanol/water (90:10:1, v/v/v) or chloroform/methanol (9:1 or 95:5, v/v) and sprayed with orcinol/sulfuric acid vapor prior to revelation by charring.

Glycolipid Purification. *1-TLC.* For preparative TLC, 150 μL of glycolipid sample was spotted on a 150 mm band on a 60 μm silica gel plate with a glass back (20 cm × 20 cm) and migrated in a solution of chloroform/methanol/water (90:10:1, v/v/v). Plate sides were sprayed with orcinol in 20% sulfuric acid and charred to reveal glycolipids while the plate center was reversibly colored with iodide vapor.

2-Flash Chromatography. Glycolipid extracts were impregnated with silica gel overnight. After an equilibration step, impregnated silica was added on top of a low-pressure silica gel column (15 μm, 4 g; Interchim, France) and a linear gradient started on Puriflash (Interchim, France) from 100% chloroform to reach 85% chloroform/15% methanol at 20 min. This ratio was maintained for 10 min. Six milliliter fractions were collected during the gradient phase, and the presence of glycolipids was checked by TLC. Fractions containing GPL were pooled, dried, and dissolved in chloroform/methanol (2:1, v/v).

GPL Saponification and Methanolysis. Ten microliters of purified GPL was dried under nitrogen; 200 μL of sodium hydroxide (0.1 M) in chloroform/methanol (2:1, v/v) was added and heated for 2 h at 37 °C. After the reaction, 1 mL of chloroform and 1 mL of water were added. The mixture was vortexed for 1 min and then centrifuged for 30 s. The lower chloroform phase was dried under nitrogen and dissolved in 150 μL of chloroform/methanol (2:1, v/v). For methanolysis, 10 μL of purified GPL was dried under nitrogen and desiccated overnight; then, 200 μL of methanol/HCl 0.5 N was added and heated overnight at 100 °C. After the reaction, 1 mL of chloroform and 1 mL of water were added. The mixture was vortexed for 1 min and centrifuged for 30 s, and the lower chloroform phase was dried under nitrogen and dissolved in 250 μL of heptane.

https://dx.doi.org/10.1021/acsinfecdis.0c00490
ACS Infect. Dis. 2020, 6, 2756−2770

Itol-acetate Derivatives. For the hydrolysis step, 1 μg of mesoinositol, 20 μL of GPL fraction, and 1 mL of TFA (3 M) were mixed, then heated for 4 h at 80 °C, dried, and desiccated overnight. The reduction step was conducted for 4 h at room temperature in 500 μL of $NaBH_4$ (10 mg/mL) in 2 M NH_4. The reaction was stopped with concentrated glacial acetic acid. Samples were dried at 55 °C under a nitrogen stream by codistillation with methanol/acetic acid three times, desiccated overnight, and incubated in 500 μL of acetic anhydride for 4 h at 80 °C. The reaction products were extracted several times with chloroform/water. The chloroform-rich phase was then filtered, dried, and dissolved in 100 μL of chloroform. Similar experiments were conducted using Rha or 6-dTal standards (Carbosynth, UK).

MALDI-TOF Mass Spectrometry. Before 5 μL was spotted on the MALDI plate with a glass capillary tube, 5 μL of 10 mg/mL dihydroxybenzoïc acid (DHB) in chloroform/methanol (1:2, v/v) was mixed with 5 μL of the sample extract in chloroform/methanol (2:1, v/v). MS and MS^n spectra were acquired on an Axima Resonance (Shimadzu Kyoto, Japan) in reflectron mode. For MS^2 experiments, collision energy was tuned from 300 to 600 eV. For MS^3, ion selection occurred with standard resolution with the same collision energy.

GC-MS Analysis. *1-Itol-acetates.* One microliter of itol-acetate derivatives was injected in splitless mode on a Solgel 1 MS, 30 m × 0.25 mm × 0.25 μm capillary column with the following gradient temperature: 120 to 230 °C at 3 °C/min and then to 270 °C at 10 °C/min. Compounds were detected after electronic impact at 70 eV on a HP-7820 gas chromatograph coupled to a 5976 single quad (Agilent Technologies, Santa Clara, US) in full scan mode from 50 to 500 Da.

2-FAMEs and TMS Derivatives. After methanolysis, released FAMEs were extracted in heptane and analyzed on a TRACE 1300 gas chromatograph coupled to an ISQ single quad (Thermo Fisher Scientific, San Jose, US). One microliter was injected in splitless mode on a SLB-5 MS, 30 m × 0.25 mm × 0.25 μm capillary column with the following gradient temperature: 50 to 140 °C at 10 °C/min and then to 310 °C at 15 °C/min. After electronic impact at 70 eV, spectra were acquired simultaneously in selected ion monitoring at 74 and 87 Da and in full scan mode from 50 to 700 Da. Trimethylsilyl derivatives of FAMEs were produced by adding 100 μL of BSTFA (N,O-bis(trimethylsilyl)trifluoroacetamide)- and 100 μL of pyridine. After 2 h at room temperature, 300 μL of heptane was added and processed using the same conditions as for FAMEs. A methyl 3-hydroxy octadecanoate (Matreya, US) was also submitted to TMS derivation to check the fragmentation model.

Nuclear Magnetic Resonance. Flash purified GPL were dried and dissolved in a mixture of $CDCl_3/CD_3OD$ (2:1, v/v) with 0.03% trimethylsilane (Eurisotop, France) three times and then dissolved in a final volume of 200 μL. The sample was then introduced into a 3 mm glass tube (Shigemi, Allison Park, PA, US). A TBI probe was used to observe ^1H and ^{13}C nuclei at 293 K on an AVANCE II system (Bruker Biospin GmbH, Germany). Impulsion sequences used for homonuclear and heteronuclear experiments were from the manufacturer. After acquisition, phase correction and calibration on trimethylsilane signals were performed for δ ^1H and δ ^{13}C. For HSQC, calibration was adjusted on the methanol signal.

Statistical Analyses. Statistical analyses were performed on Prism 5.0 (Graphpad) or in R studio (for AFM experiments) and detailed for each figure legend: $*p < 0.05$; $**p < 0.01$; $***p < 0.001$.

■ ASSOCIATED CONTENT

Supporting Information

The Supporting Information is available free of charge at https://pubs.acs.org/doi/10.1021/acsinfecdis.0c00490.

Table S1: List of primers used in this study; Table S2: List of bacterial strains used in this study; Table S3: List of plasmids used in this study; Figure S1: Monosaccharide analysis of purified diglycosylated GPL; Figure S2: Monosaccharide analysis of purified triglycosylated GPL; Figure S3: MS/MS sequencing of GPL-3; Figure S4: MS/MS sequencing of saponified WT GPL-3; Figure S5: MS^3 investigation of m/z 1038 fragment; Figure S6: Analysis of Δ*fmt* strains overproducing Fmt(G86A), Fmt(G88A), or Fmt(G86A/G88A); Figure S7: MS^3 analysis of the Δ*fmt* strain transformed with pMV306-*fmt*-G88A, pMV306-*fmt*-G86A, or pMV306-*fmt*-G86A/G88A; Figure S8: Atomic force microscopy with hydrophobic probes (PDF)

■ AUTHOR INFORMATION

Corresponding Author

Laurent Kremer − *Centre National de la Recherche Scientifique UMR 9004, Institut de Recherche en Infectiologie de Montpellier (IRIM), Université de Montpellier, 34293 Montpellier, France; INSERM, IRIM, 34293 Montpellier, France;* orcid.org/0000-0002-6604-4458; Phone: (+33) 4 34 35 94 47; Email: laurent.kremer@irim.cnrs.fr

Authors

Wassim Daher − *Centre National de la Recherche Scientifique UMR 9004, Institut de Recherche en Infectiologie de Montpellier (IRIM), Université de Montpellier, 34293 Montpellier, France; INSERM, IRIM, 34293 Montpellier, France*

Louis-David Leclercq − *Univ. Lille, CNRS, UMR 8576 - UGSF - Unité de Glycobiologie Structurale et Fonctionnelle, F-59000 Lille, France*

Albertus Viljoen − *Centre National de la Recherche Scientifique UMR 9004, Institut de Recherche en Infectiologie de Montpellier (IRIM), Université de Montpellier, 34293 Montpellier, France; Louvain Institute of Biomolecular Science and Technology, Université Catholique de Louvain, B-1348 Louvain-la-Neuve, Belgium*

Jona Karam − *Centre National de la Recherche Scientifique UMR 9004, Institut de Recherche en Infectiologie de Montpellier (IRIM), Université de Montpellier, 34293 Montpellier, France*

Yves F. Dufrêne − *Louvain Institute of Biomolecular Science and Technology, Université Catholique de Louvain, B-1348 Louvain-la-Neuve, Belgium;* orcid.org/0000-0002-7289-4248

Yann Guérardel − *Univ. Lille, CNRS, UMR 8576 - UGSF - Unité de Glycobiologie Structurale et Fonctionnelle, F-59000 Lille, France;* orcid.org/0000-0003-4967-9512

Complete contact information is available at: https://pubs.acs.org/10.1021/acsinfecdis.0c00490

https://dx.doi.org/10.1021/acsinfecdis.0c00490
ACS Infect. Dis. 2020, 6, 2756−2770

Author Contributions

[‖]W.D. and L.-D.L. contributed equally to this work. W.D. conceived and conducted experiments, analyzed the data, and wrote the manuscript. L.-D.L., A.V., and J.K. conducted the experiments. L.-D.L., A.V., Y.F.D., Y.G., and L.K. analyzed the data and participated in writing the manuscript. L.K. conceived the idea of the project and wrote the manuscript.

Notes

The funders had no role in the study design, data collection, interpretation, or decision to submit the work for publication. The authors declare no competing financial interest.

■ ACKNOWLEDGMENTS

We are indebted to the PAGés platform (http://plateforme-pages.univ-lille1.fr) and UMS 2014 - US 41 - Plateformes Lilloises en Biologie & Santé for providing the scientific and technical environment conducive to achieving this work. Y.F.D. is the Research Director at the FNRS. This work was supported by the Fondation pour la Recherche Médicale (FRM) [grant number DEQ20150331719] to L.K. and the National Research Agency grant ANR-19-CE15-0012-01 (SUNLIVE) to L.K. and Y.G. We acknowledge the Infectiopôle Sud Méditerranée for funding the PhD fellowship of J.K. Work at UCLouvain was supported by the Excellence of Science-EOS programme (Grant #30550343), the European Research Council (ERC) under the European Union's Horizon 2020 research and innovation program (grant agreement no. 693630), the FNRS-WELBIO (grant no. WELBIO-CR-2015A-05), the National Fund for Scientific Research (FNRS), and the Research Department of the Communauté française de Belgique (Concerted Research Action).

■ REFERENCES

(1) Johansen, M. D., Herrmann, J.-L., and Kremer, L. (2020) Non-Tuberculous Mycobacteria and the Rise of *Mycobacterium abscessus*. *Nat. Rev. Microbiol. 18*, 392−407.

(2) Brown-Elliott, B. A., Nash, K. A., and Wallace, R. J. (2012) Antimicrobial Susceptibility Testing, Drug Resistance Mechanisms, and Therapy of Infections with Nontuberculous Mycobacteria. *Clin. Microbiol. Rev. 25*, 545−582.

(3) Esther, C. R., Esserman, D. A., Gilligan, P., Kerr, A., and Noone, P. G. (2010) Chronic *Mycobacterium abscessus* Infection and Lung Function Decline in Cystic Fibrosis. *J. Cystic Fibrosis 9*, 117−123.

(4) Sermet-Gaudelus, I., Le Bourgeois, M., Pierre-Audigier, C., Offredo, C., Guillemot, D., Halley, S., Akoua-Koffi, C., Vincent, V., Sivadon-Tardy, V., Ferroni, A., Berche, P., Scheinmann, P., Lenoir, G., and Gaillard, J.-L. (2003) *Mycobacterium abscessus* and Children with Cystic Fibrosis. *Emerging Infect. Dis. 9*, 1587−1591.

(5) Howard, S. T., Rhoades, E., Recht, J., Pang, X., Alsup, A., Kolter, R., Lyons, C. R., and Byrd, T. F. (2006) Spontaneous Reversion of *Mycobacterium abscessus* from a Smooth to a Rough Morphotype Is Associated with Reduced Expression of Glycopeptidolipid and Reacquisition of an Invasive Phenotype. *Microbiology (London, U. K.) 152*, 1581−1590.

(6) Medjahed, H., Gaillard, J.-L., and Reyrat, J.-M. (2010) *Mycobacterium abscessus*: A New Player in the Mycobacterial Field. *Trends Microbiol. 18*, 117−123.

(7) Gutiérrez, A. V., Viljoen, A., Ghigo, E., Herrmann, J.-L., and Kremer, L. (2018) Glycopeptidolipids, a Double-Edged Sword of the *Mycobacterium abscessus* Complex. *Front. Microbiol. 9*, 1145.

(8) Pawlik, A., Garnier, G., Orgeur, M., Tong, P., Lohan, A., Le Chevalier, F., Sapriel, G., Roux, A. L., Conlon, K., Honoré, N., Dillies, M. A., Ma, L., Bouchier, C., Coppée, J. Y., Gaillard, J. L., Gordon, S. V., Loftus, B., Brosch, R., and Herrmann, J. L. (2013) Identification and Characterization of the Genetic Changes Responsible for the Characteristic Smooth-to-Rough Morphotype Alterations of Clinically Persistent *Mycobacterium abscessus*. *Mol. Microbiol. 90*, 612−629.

(9) Catherinot, E., Roux, A.-L., Macheras, E., Hubert, D., Matmar, M., Dannhoffer, L., Chinet, T., Morand, P., Poyart, C., Heym, B., Rottman, M., Gaillard, J.-L., and Herrmann, J.-L. (2009) Acute Respiratory Failure Involving an R Variant of *Mycobacterium abscessus*. *J. Clin. Microbiol. 47*, 271−274.

(10) Jönsson, B. E., Gilljam, M., Lindblad, A., Ridell, M., Wold, A. E., and Welinder-Olsson, C. (2007) Molecular Epidemiology of *Mycobacterium abscessus* with Focus on Cystic Fibrosis. *J. Clin. Microbiol. 45*, 1497−1504.

(11) Ryan, K., and Byrd, T. F. (2018) *Mycobacterium abscessus*: Shapeshifter of the Mycobacterial World. *Front. Microbiol. 9*, 2642.

(12) Madani, A., Ridenour, J. N., Martin, B. P., Paudel, R. R., Abdul Basir, A., Le Moigne, V., Herrmann, J.-L., Audebert, S., Camoin, L., Kremer, L., Spilling, C. D., Canaan, S., and Cavalier, J.-F. (2019) Cyclipostins and Cyclophostin Analogues as Multitarget Inhibitors That Impair Growth of *Mycobacterium abscessus*. *ACS Infect. Dis. 5*, 1597−1608.

(13) Bernut, A., Viljoen, A., Dupont, C., Sapriel, G., Blaise, M., Bouchier, C., Brosch, R., de Chastellier, C., Herrmann, J.-L., and Kremer, L. (2016) Insights into the Smooth-to-Rough Transitioning in *Mycobacterium bolletii* Unravels a Functional Tyr Residue Conserved in All Mycobacterial MmpL Family Members. *Mol. Microbiol. 99*, 866−883.

(14) Viljoen, A., Gutiérrez, A. V., Dupont, C., Ghigo, E., and Kremer, L. A. (2018) Simple and Rapid Gene Disruption Strategy in *Mycobacterium abscessus*: On the Design and Application of Glycopeptidolipid Mutants. *Front. Cell. Infect. Microbiol. 8*, 69.

(15) Viljoen, A., Viela, F., Kremer, L., and Dufrêne, Y. F. (2020) Fast Chemical Force Microscopy Demonstrates That Glycopeptidolipids Define Nanodomains of Varying Hydrophobicity on Mycobacteria. *Nanoscale Horiz. 5*, 944−953.

(16) Bernut, A., Herrmann, J.-L., Kissa, K., Dubremetz, J.-F., Gaillard, J.-L., Lutfalla, G., and Kremer, L. (2014) *Mycobacterium abscessus* Cording Prevents Phagocytosis and Promotes Abscess Formation. *Proc. Natl. Acad. Sci. U. S. A. 111*, E943−952.

(17) Roux, A.-L., Viljoen, A., Bah, A., Simeone, R., Bernut, A., Laencina, L., Deramaudt, T., Rottman, M., Gaillard, J.-L., Majlessi, L., Brosch, R., Girard-Misguich, F., Vergne, I., de Chastellier, C., Kremer, L., and Herrmann, J.-L. (2016) The Distinct Fate of Smooth and Rough *Mycobacterium abscessus* Variants inside Macrophages. *Open Biol. 6*, 160185.

(18) Whang, J., Back, Y. W., Lee, K.-I., Fujiwara, N., Paik, S., Choi, C. H., Park, J.-K., and Kim, H.-J. (2017) *Mycobacterium abscessus* Glycopeptidolipids Inhibit Macrophage Apoptosis and Bacterial Spreading by Targeting Mitochondrial Cyclophilin D. *Cell Death Dis. 8*, No. e3012.

(19) Roux, A.-L., Ray, A., Pawlik, A., Medjahed, H., Etienne, G., Rottman, M., Catherinot, E., Coppée, J.-Y., Chaoui, K., Monsarrat, B., Toubert, A., Daffé, M., Puzo, G., Gaillard, J.-L., Brosch, R., Dulphy, N., Nigou, J., and Herrmann, J.-L. (2011) Overexpression of Proinflammatory TLR-2-Signalling Lipoproteins in Hypervirulent Mycobacterial Variants. *Cell. Microbiol. 13*, 692−704.

(20) Bernut, A., Herrmann, J.-L., Ordway, D., and Kremer, L. (2017) The Diverse Cellular and Animal Models to Decipher the Physiopathological Traits of *Mycobacterium abscessus* Infection. *Front. Cell. Infect. Microbiol. 7*, 100.

(21) Catherinot, E., Clarissou, J., Etienne, G., Ripoll, F., Emile, J.-F., Daffé, M., Perronne, C., Soudais, C., Gaillard, J.-L., and Rottman, M. (2007) Hypervirulence of a Rough Variant of the *Mycobacterium abscessus* Type Strain. *Infect. Immun. 75*, 1055−1058.

(22) Bernut, A., Dupont, C., Sahuquet, A., Herrmann, J.-L., Lutfalla, G., and Kremer, L. (2015) Deciphering and Imaging Pathogenesis and Cording of *Mycobacterium abscessus* in Zebrafish Embryos. *J. Visualized Exp. 103*, No. e53130.

https://dx.doi.org/10.1021/acsinfecdis.0c00490
ACS Infect. Dis. 2020, 6, 2756−2770

(23) Jankute, M., Cox, J. A. G., Harrison, J., and Besra, G. S. (2015) Assembly of the Mycobacterial Cell Wall. *Annu. Rev. Microbiol. 69*, 405−423.
(24) Brennan, P. J., and Nikaido, H. (1995) The Envelope of Mycobacteria. *Annu. Rev. Biochem. 64*, 29−63.
(25) Schorey, J. S., and Sweet, L. (2008) The Mycobacterial Glycopeptidolipids: Structure, Function, and Their Role in Pathogenesis. *Glycobiology 18*, 832−841.
(26) Ripoll, F., Deshayes, C., Pasek, S., Laval, F., Beretti, J.-L., Biet, F., Risler, J.-L., Daffé, M., Etienne, G., Gaillard, J.-L., and Reyrat, J.-M. (2007) Genomics of Glycopeptidolipid Biosynthesis in *Mycobacterium abscessus* and *M. chelonae*. *BMC Genomics 8*, 114.
(27) Burbaud, S., Laval, F., Lemassu, A., Daffé, M., Guilhot, C., and Chalut, C. (2016) Trehalose Polyphleates Are Produced by a Glycolipid Biosynthetic Pathway Conserved across Phylogenetically Distant Mycobacteria. *Cell. Chem. Biol. 23*, 278−289.
(28) Vats, A., Singh, A. K., Mukherjee, R., Chopra, T., Ravindran, M. S., Mohanty, D., Chatterji, D., Reyrat, J.-M., and Gokhale, R. S. (2012) Retrobiosynthetic Approach Delineates the Biosynthetic Pathway and the Structure of the Acyl Chain of Mycobacterial Glycopeptidolipids. *J. Biol. Chem. 287*, 30677−30687.
(29) Villeneuve, C., Etienne, G., Abadie, V., Montrozier, H., Bordier, C., Laval, F., Daffé, M., Maridonneau-Parini, I., and Astarie-Dequeker, C. (2003) Surface-Exposed Glycopeptidolipids of *Mycobacterium smegmatis* Specifically Inhibit the Phagocytosis of Mycobacteria by Human Macrophages. Identification of a Novel Family of Glycopeptidolipids. *J. Biol. Chem. 278*, 51291−51300.
(30) Ojha, A. K., Varma, S., and Chatterji, D. (2002) Synthesis of an unusual polar glycopeptidolipid in glucose-limited culture of *Mycobacterium smegmatis*. *Microbiology 148*, 3039−3048.
(31) Deshayes, C., Laval, F., Montrozier, H., Daffé, M., Etienne, G., and Reyrat, J.-M. A. (2005) Glycosyltransferase Involved in Biosynthesis of Triglycosylated Glycopeptidolipids in *Mycobacterium smegmatis*: Impact on Surface Properties. *J. Bacteriol. 187*, 7283−7291.
(32) Wiersma, C., Belardinelli, J. M., Avanzi, C., Angala, S. K., Everall, I., Angala, B., Kendall, E., Moura, V., Verma, D., Benoit, J., Brown, K., Jones, V., Malcom, K., Strong, M., Nick, J., Floto, R. A., Parkhill, J., Ordway, D., Davidson, R., McNeil, M. R., and Jackson, M. C. (2020) Cell Surface Remodeling of *Mycobacterium abscessus* under Cystic Fibrosis Airway Growth Conditions. *ACS Infect. Dis. 6*, 2143−2154.
(33) Sweet, L., Zhang, W., Torres-Fewell, H., Serianni, A., Boggess, W., and Schorey, J. (2008) *Mycobacterium avium* Glycopeptidolipids Require Specific Acetylation and Methylation Patterns for Signaling through Toll-like Receptor 2. *J. Biol. Chem. 283*, 33221−33231.
(34) Billman-Jacobe, H., McConville, M. J., Haites, R. E., Kovacevic, S., and Coppel, R. L. (1999) Identification of a Peptide Synthetase Involved in the Biosynthesis of Glycopeptidolipids of *Mycobacterium smegmatis*. *Mol. Microbiol. 33*, 1244−1253.
(35) Sondén, B., Kocíncová, D., Deshayes, C., Euphrasie, D., Rhayat, L., Laval, F., Frehel, C., Daffé, M., Etienne, G., and Reyrat, J.-M. (2005) Gap, a Mycobacterial Specific Integral Membrane Protein, Is Required for Glycolipid Transport to the Cell Surface. *Mol. Microbiol. 58*, 426−440.
(36) Jeevarajah, D., Patterson, J. H., Taig, E., Sargeant, T., McConville, M. J., and Billman-Jacobe, H. (2004) Methylation of GPLs in *Mycobacterium smegmatis* and *Mycobacterium avium*. *J. Bacteriol. 186*, 6792−6799.
(37) Richard, M., Gutiérrez, A. V., Viljoen, A., Rodriguez-Rincon, D., Roquet-Banères, F., Blaise, M., Everall, I., Parkhill, J., Floto, R. A., and Kremer, L. (2019) Mutations in the MAB_2299c TetR Regulator Confer Cross-Resistance to Clofazimine and Bedaquiline in *Mycobacterium abscessus*. *Antimicrob. Agents Chemother. 63*, No. e01316-18.
(38) Lee, M. H., Pascopella, L., Jacobs, W. R., and Hatfull, G. F. (1991) Site-Specific Integration of Mycobacteriophage L5: Integration-Proficient Vectors for *Mycobacterium smegmatis Mycobacterium tuberculosis* and Bacille Calmette-Guérin. *Proc. Natl. Acad. Sci. U. S. A. 88*, 3111−3115.
(39) Gao, J., and Sampson, N. S. (2014) A GMC Oxidoreductase Homologue Is Required for Acetylation of Glycopeptidolipid in *Mycobacterium smegmatis*. *Biochemistry 53*, 611−613.
(40) Lopez-Marin, L. M., Gautier, N., Lanéelle, M.-A., Silve, G., and Daffe, M. (1994) Structures of the Glycopeptidolipid Antigens of *Mycobacterium abscessus* and *Mycobacterium chelonae* and Possible Chemical Basis of the Serological Cross-Reactions in the *Mycobacterium fortuitum* Complex. *Microbiology 140*, 1109−1118.
(41) López Marin, L. M., Lanéelle, M. A., Promé, D., Daffé, M., Lanéelle, G., and Promé, J. C. (1991) Glycopeptidolipids from *Mycobacterium fortuitum*: A Variant in the Structure of C-Mycoside. *Biochemistry 30*, 10536−10542.
(42) Keller, J. P., Smith, P. M., Benach, J., Christendat, D., deTitta, G. T., and Hunt, J. F. (2002) The Crystal Structure of MT0146/CbiT Suggests That the Putative Precorrin-8w Decarboxylase Is a Methyltransferase. *Structure 10*, 1475−1487.
(43) Rainczuk, A. K., Klatt, S., Yamaryo-Botté, Y., Brammananth, R., McConville, M. J., Coppel, R. L., and Crellin, P. K. (2020) MtrP, A Putative Methyltransferase in *Corynebacteria* Is Required for Optimal Membrane Transport of Trehalose Mycolates. *J. Biol. Chem. 295*, 6108−6119.
(44) Pérez, E., Constant, P., Laval, F., Lemassu, A., Lanéelle, M.-A., Daffé, M., and Guilhot, C. (2004) Molecular Dissection of the Role of Two Methyltransferases in the Biosynthesis of Phenolglycolipids and Phthiocerol Dimycoserosate in the *Mycobacterium tuberculosis* Complex. *J. Biol. Chem. 279*, 42584−42592.
(45) Jeevarajah, D., Patterson, J. H., McConville, M. J., and Billman-Jacobe, H. (2002) Modification of Glycopeptidolipids by an *O*-Methyltransferase of *Mycobacterium smegmatis*. *Microbiology (London, U. K.) 148*, 3079−3087.
(46) Jankute, M., Nataraj, V., Lee, O. Y.-C., Wu, H. H. T., Ridell, M., Garton, N. J., Barer, M. R., Minnikin, D. E., Bhatt, A., and Besra, G. S. (2017) The Role of Hydrophobicity in Tuberculosis Evolution and Pathogenicity. *Sci. Rep. 7*, 1315.
(47) Alsteens, D., Dague, E., Rouxhet, P. G., Baulard, A. R., and Dufrêne, Y. F. (2007) Direct Measurement of Hydrophobic Forces on Cell Surfaces Using AFM. *Langmuir 23*, 11977−11979.
(48) Doyle, R. J. (2000) Contribution of the Hydrophobic Effect to Microbial Infection. *Microbes Infect. 2*, 391−400.
(49) Minnikin, D. E., Lee, O. Y.-C., Wu, H. H. T., Besra, G. S., Bhatt, A., Nataraj, V., Rothschild, B. M., Spigelman, M., and Donoghue, H. D. (2015) Ancient Mycobacterial Lipids: Key Reference Biomarkers in Charting the Evolution of Tuberculosis. *Tuberculosis (Oxford, U. K.) 95*, S133−139.
(50) Johansen, M. D., and Kremer, L. (2020) A Zebrafish Model of *Mycobacterium kansasii* Infection Reveals Large Extracellular Cord Formation. *J. Infect. Dis. 222*, 1046−1050.
(51) Alsteens, D., Verbelen, C., Dague, E., Raze, D., Baulard, A. R., and Dufrêne, Y. F. (2008) Organization of the Mycobacterial Cell Wall: A Nanoscale View. *Pfluegers Arch. 456*, 117−125.
(52) Dague, E., Alsteens, D., Latgé, J.-P., Verbelen, C., Raze, D., Baulard, A. R., and Dufrêne, Y. F. (2007) Chemical Force Microscopy of Single Live Cells. *Nano Lett. 7*, 3026−3030.
(53) Arbues, A., Lugo-Villarino, G., Neyrolles, O., Guilhot, C., and Astarie-Dequeker, C. (2014) Playing Hide-and-Seek with Host Macrophages through the Use of Mycobacterial Cell Envelope Phthiocerol Dimycocerosates and Phenolic Glycolipids. *Front. Cell. Infect. Microbiol. 4*, 173.
(54) Etienne, G., Villeneuve, C., Billman-Jacobe, H., Astarie-Dequeker, C., Dupont, M.-A., and Daffé, M. (2002) The Impact of the Absence of Glycopeptidolipids on the Ultrastructure, Cell Surface and Cell Wall Properties, and Phagocytosis of *Mycobacterium smegmatis*. *Microbiology 148*, 3089−3100.
(55) Bartley, S. N., Tzeng, Y.-L., Heel, K., Lee, C. W., Mowlaboccus, S., Seemann, T., Lu, W., Lin, Y.-H., Ryan, C. S., Peacock, C., Stephens, D. S., Davies, J. K., and Kahler, C. M. (2013) Attachment and Invasion of *Neisseria meningitidis* to Host Cells Is Related to Surface Hydrophobicity, Bacterial Cell Size and Capsule. *PLoS One 8*, No. e55798.

https://dx.doi.org/10.1021/acsinfecdis.0c00490
ACS Infect. Dis. 2020, 6, 2756−2770

(56) Araújo, A. M. M., Oliveira, I. C. M. de, Mattos, M. C. de, and Benchetrit, L. C. (2008) Cell Surface Hydrophobicity and Adherence of a Strain of Group B *Streptococci* during the Post-Antibiotic Effect of Penicillin. *Rev. Inst. Med. Trop. Sao Paulo 50*, 203−207.
(57) Horstmann, J. A., Lunelli, M., Cazzola, H., Heidemann, J., Kühne, C., Steffen, P., Szefs, S., Rossi, C., Lokareddy, R. K., Wang, C., Lemaire, L., Hughes, K. T., Uetrecht, C., Schlüter, H., Grassl, G. A., Stradal, T. E. B., Rossez, Y., Kolbe, M., and Erhardt, M. (2020) Methylation of *Salmonella typhimurium* Flagella Promotes Bacterial Adhesion and Host Cell Invasion. *Nat. Commun. 11*, 2013.
(58) Viljoen, A., Blaise, M., de Chastellier, C., and Kremer, L. (2016) MAB_3551c Encodes the Primary Triacylglycerol Synthase Involved in Lipid Accumulation in *Mycobacterium abscessus*. *Mol. Microbiol. 102*, 611−627.
(59) Hutter, J. L., and Bechhoefer, J. (1993) Calibration of Atomic-force Microscope Tips. *Rev. Sci. Instrum. 64*, 1868−1873.
(60) Raynaud, C., Daher, W., Johansen, M., Roquet-Banères, F., Blaise, M., Onajole, O. K., Kozikowski, A., Herrmann, J.-L., Dziadek, J., Gobis, K., and Kremer, L. (2020) Active Benzimidazole Derivatives Targeting the MmpL3 Transporter in *Mycobacterium abscessus*. *ACS Infect. Dis. 6*, 324−337.

https://dx.doi.org/10.1021/acsinfecdis.0c00490
ACS Infect. Dis. 2020, 6, 2756−2770